Applied Energy 377 (2025) 124702

Contents lists available at ScienceDirect

Applied Energy

journal homepage: www.elsevier.com/locate/apenergy

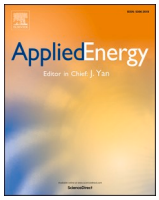

DOMES: A general optimization method for the integrated design of energy conversion, storage and networks in multi-energy systems

Enrico Dal Cin [a,*], Gianluca Carraro [a], Gabriele Volpato [a], Andrea Lazzaretto [a], George Tsatsaronis [b]

[a] University of Padova, Industrial Engineering Department, Via Venezia 1, 35121 Padova, Italy
[b] Technische Universität Berlin, Chair of Energy Engineering and Environmental Protection, Marchstrasse 18, 10587 Berlin, Germany

HIGHLIGHTS

- Optimal synthesis, design and operation of multi-energy systems including networks.
- Development of a two-level evolutionary algorithm with a MILP sub-problem.
- Decomposition of the topological optimization from the design and operation problem.
- Design from scratch of new multi-energy systems or retrofit of existing ones.
- Single or multi-objective optimization to minimize total costs and carbon emissions.

GRAPHICAL ABSTRACT

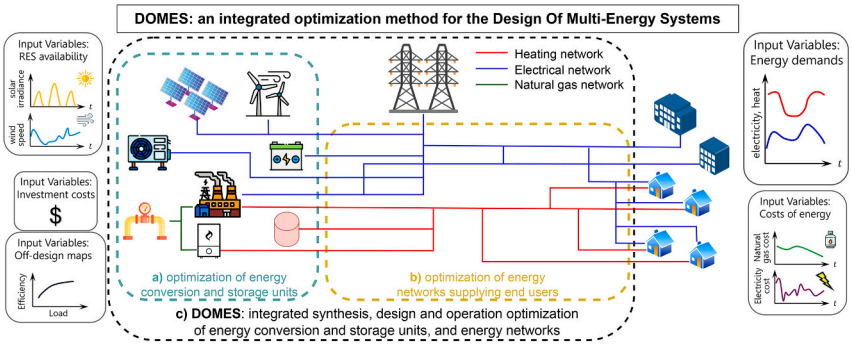

ARTICLE INFO

Keywords:
Decarbonization
Decomposition
District heating network
Microgrid
MILP
Multi-objective optimization

ABSTRACT

A realistic pursuit of decarbonization targets requires planning and designing new configurations of "multi-energy systems" to identify the optimal number, type, location and size of the energy conversion and storage units and their interconnections with the end users of different forms of energy. The common approach in the literature is to treat the optimization problem of energy conversion and storage separately from that of energy networks, and the few attempts to address the two problems simultaneously have led to oversimplifications due to the very large number of decision variables involved. To fill this gap, this study introduces "*DOMES*" (*Design Of Multi-Energy Systems*), a general optimization method for the integrated synthesis, design and operation of a multi-energy system in its entirety. With the goal of minimizing costs and reducing carbon emissions, DOMES can simultaneously find the location, type, size and operation of the energy conversion and storage units, as well as the topology and capacity of the energy networks, to meet the energy demand of the end users. To make the problem computationally solvable while ensuring sufficiently good accuracy of the solution, mathematical techniques such as linearization, problem decomposition and time series aggregation have been applied. DOMES is capable of finding the global optimum of the problem either while planning new systems from scratch or when starting from existing systems. Considering a densely populated urban district, the investment costs of renewable conversion plants outweigh those of the district heating network and electric microgrid, which together account for less than 10 % of the total. A much higher economic impact of energy networks is expected when considering larger, less densely populated areas.

* Corresponding author.
E-mail addresses: enrico.dalcin@phd.unipd.it (E. Dal Cin), gianluca.carraro@unipd.it (G. Carraro), gabriele.volpato.1@phd.unipd.it (G. Volpato), andrea.lazzaretto@unipd.it (A. Lazzaretto), georgios.tsatsaronis@tu-berlin.de (G. Tsatsaronis).

https://doi.org/10.1016/j.apenergy.2024.124702
Received 10 June 2024; Received in revised form 6 September 2024; Accepted 10 October 2024
Available online 23 October 2024

Nomenclature

Abbreviations

CHP	combined heat and power
DHN	district heating network
EA	evolutionary algorithm
EES	electric energy storage
EMG	electrical microgrid
GB	gas boiler
HP	heat pump
IR	intermediate representation
MES	multi-energy system
MILP	mixed integer linear programming
MINLP	mixed integer nonlinear programming
PV	photovoltaic
OR	optimal representation
SDO	synthesis, design and operation
SOC	state of charge
SR	starting representation
TD	typical day
TES	thermal energy storage

Sets

C	dispatchable energy conversion technologies
D	days of a year
E	energy carriers
I	generation of individuals
K	typical days (clusters)
N	nodes of the system
P	population of individuals
R	non-dispatchable energy conversion technologies
S	energy storage technologies
T	hourly time steps of a day

Subscripts

c	dispatchable energy conversion technology, $c \in C$
d	day of the year, $d \in D = \{1, 2, \ldots, 365\}$
e	energy carrier, $e \in E$
j	current iteration
k	typical day or cluster centre, $k \in K$
m	node, $m \in N$
n	node, $n \in N$
r	non-dispatchable energy conversion technology, $r \in R$
s	energy storage technology, $s \in S$
t	time step of a day, $t \in T = \{1, 2, \ldots, 24\}$

Superscripts

best	best individual
cap	capital cost
char	charging phase
disc	discharging phase
end	final set of individuals of a generation
exc	import/export exchange permission
exp	export
imp	import
inter	inter-day state of charge
intra	intra-day state of charge
max	maximum value
mid	intermediate set of individuals of a generation
min	minimum value
net	energy network
off	offspring generation
oper	operating cost
par	parent generation
sel	selected part of a population
start	starting set of individuals of a generation
worst	worst individual
0	no upper limit on CO_2 emissions

Roman symbols

a	number of individuals of parent generations, positive integer number
b	termination threshold of the evolutionary algorithm, dimensionless
f	objective function, $€$
g	map function that associates any day of the year to its typical day, function
h	timestep size, 1 h
i	individual, mathematical object
J	maximum number of iterations of the evolutionary algorithm, positive integer number
l	distance between two nodes, m
M	large enough value for big-M constraints, positive real number
q	fitness value, $€$
w	weight of a typical day, number of days represented
x	geographical coordinate (abscissa), m
y	geographical coordinate (ordinate), m

Greek symbols

α	size-specific investment cost, $€/kW$, $€/kWh$ or $€/kW/m$
β	fixed investment cost, $€$ or $€/m$
γ	specific cost/price of a carrier, $€/kWh$
Δ	synthesis binary variable, $\Delta \in \{0, 1\}$
δ	operational binary variable (on/off state), $\delta \in \{0, 1\}$
ε	epsilon constraint, dimensionless
Z	rated capacity, kW or kWh
ζ	specific emission factor, kg/kWh
η	dimensionless linearization coefficient of off-design performance, or efficiency
ϑ	operational auxiliary variable, kW
ι	lifetime, *years*
λ	loss factor, dimensionless or m^{-1}
μ	input power or charge power, kW
ν	relative operation and maintenance cost, dimensionless
ξ	state of charge, kWh
o	relative minimum load or charging/discharging capacity, dimensionless or kW/kWh
π	output or discharge power, kW
ρ	interest rate, dimensionless
σ	correction factor, dimensionless
τ	actualization factor, dimensionless
υ	dimensional linearization coefficient of off-design performance, kW
φ	power flow in a network line, kW
Φ	CO_2 emissions, kg
χ	power demand, kW
ψ	power import/export, kW

Other symbols

*	generic time-dependent input data

1. Introduction

The energy sector is responsible nowadays for approximately 75 % of global greenhouse gas emissions [1]. To limit global warming to 1.5 °C by the end of the century, carbon emissions must reach net zero by 2050 [2]. This calls for a paradigm shift, a transition from fossil fuels to renewable sources that must be supported by a reduction in final energy use [3]. Distributed generation, electrification and sector-coupling will be crucial aspects of this renewal [4]. There is, in fact, a growing consensus that decarbonization should not be addressed by individual sectors (electricity, heating, transportation, etc.), but requires a holistic approach aimed at developing smart energy systems that integrate multiple carriers [5]. Accordingly, in recent years researchers are increasingly focusing on multi-energy systems (MESs) [6]. A MES is an energy system of any spatial extent that involves various energy carriers (electricity, heat, fossil fuels, biomass, etc.) and provides energy in various forms to the end users [7]. It generally covers the entire supply chain from producers to consumers encompassing energy conversion, storage, delivery and end uses. How to properly design and operate a MES is among the main challenges in the implementation of such systems and fostered the development of dedicated mathematical optimization tools [8].

In general, energy system optimization can be broken down into three (not always distinct) levels: synthesis, design and operation (SDO) [9]. Synthesis refers to the layout and topology of the system, i.e., the choice of components and their interconnections. Design refers to the sizing of the chosen components and, finally, operation refers to the scheduling and management over time of components load. SDO optimization has been applied to different kinds of energy systems [10]. A non-exhaustive list of examples includes thermal power plants [10–15], bottoming thermodynamic cycles [16–20], aircraft energy systems [21], energy systems of ships [22–24], distributed energy supply systems [25,26] and MESs [27,28]. Focusing on MESs, SDO optimization problems generally fall into the category of mixed-integer nonlinear programming (MINLP), due to the presence of nonlinear relationships (e.g., off-design operation maps), binary variables (e.g., the existence of a component, or the on/off status of a component in a given time interval) and continuous variables (e.g., size of components, power flows) [29]. The need to consider a large number of components that must be designed and planned to satisfy a demand during their entire life cycle makes the search for the optimal solution extremely challenging [30]. Linearization techniques simplify the problem and convert it into a mixed integer linear programming (MILP) one [31]. The convex nature of MILP prevents the solution from falling into a local optimum and ensures that the global optimum can be found [32]. In addition, MILP is a robust approach, and many solvers are commercially available [33]. However, since the computational effort increases exponentially with increasing number of binary variables, large systems can still be computationally intractable [34].

In order for SDO models to be solvable in an acceptable time, most of the work in the literature has focused on optimizing specific aspects of a MES. Many researchers developed models to optimize the selection, placement, sizing, and operation of energy conversion and storage units that feed the users of the MES (e.g., [35–48]) (Fig. 1a). However, they considered energy networks as ideal sources/sinks from which to draw or discharge any amount of energy [35–39]. For instance, Rech et al. [37] optimized a fleet of energy conversion plants providing electrical and thermal energy to a mountain village. Heat is delivered to the end users via district heating network (DHN), which is modelled as an ideal black box collecting heat from the generators to fulfil the aggregated heating demand of the village. Alternatively, networks have been considered as given system constraints that do not require design optimization [40–48]. As an example, Wirtz [40] optimized the generation mix of a district MES including DHN of given topology and capacity. On the other hand, researchers who have worked on optimizing the layout and capacity of energy networks mostly assumed already available (mainly centralized) energy conversion plants, which do not need to be optimized (e.g., [49–52]) (Fig. 1b). For instance, Röder et al. [50]

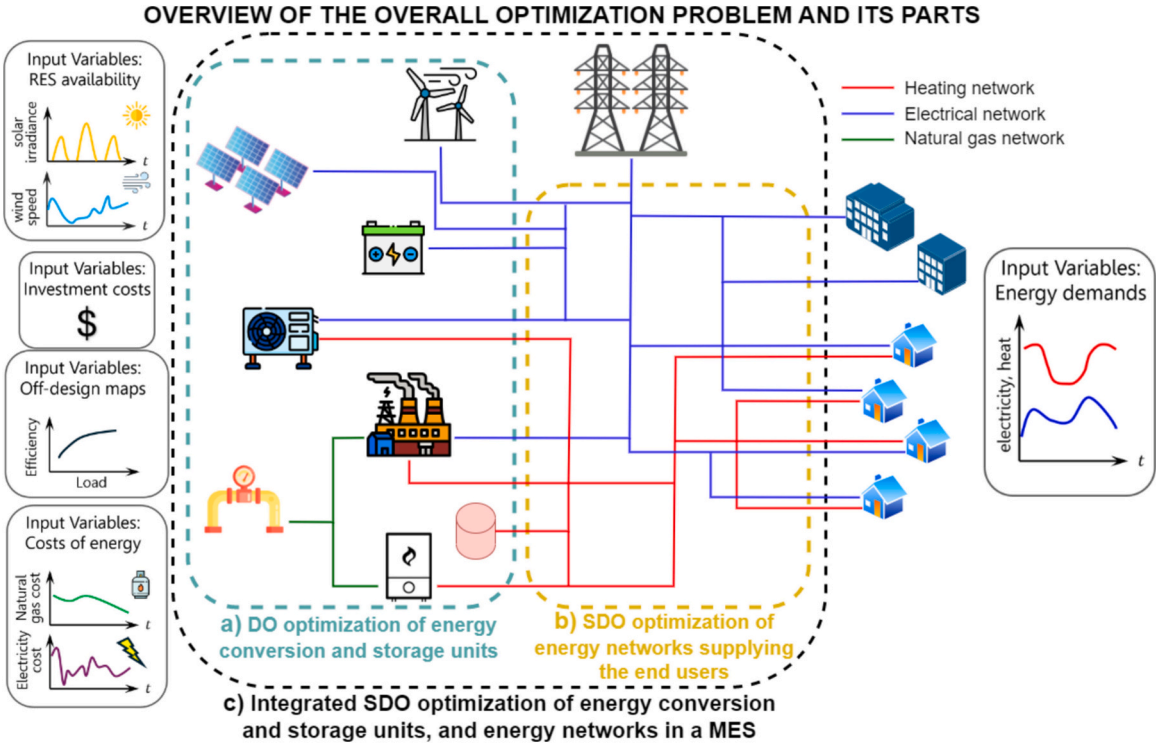

Fig. 1. Overview of different approaches for the optimization of a MES: (a) design (D) and operation (O) optimization of the energy conversion and storage units considering ideal energy networks, (b) synthesis (S), D and O optimization of the energy networks for given energy conversion and storage units, (c) integrated SDO optimization of the energy conversion and storage units, and energy networks.

optimized the topology and capacity of a German DHN but fixed in advance the design (location and capacity) of the generation and storage plants of the system. It emerges the need to develop optimization tools capable of dealing with the SDO optimization of a MES in its entirety, thereby looking for the optimal configuration of both the energy conversion and storage plants feeding the users, and the energy networks supplying them with the required energy (Fig. 1c). This integrated approach is necessary, because considering the two problems separately may lead to non-optimal solutions at the global level. In fact, optimal solutions for the design of energy conversion systems may not be optimal solutions for the system as a whole, due to the costs of interconnections with end users through energy networks.

Some tools for integrated SDO optimization of networks and plants in a MES have been proposed in the literature [53–69]. Söderman and Pettersson [53] developed a MILP model that minimizes the life cycle cost of a distributed energy system integrating DHN with combined heat and power (CHP) plants. To make the problem computationally solvable, they condensed the annual operation of the system (usually described by 8760 hourly intervals) into eight representative time intervals. Haikarainen et al. [54] proposed a similar approach to the previous one including CO_2 minimization in a multi-objective framework. Again, a year is described by very few time intervals for computational purposes. Keirstead et al. [55] also included optimization of the layout of electricity and gas networks in the SDO model of a distributed MES. To reduce the computational load, the daily operation of the system is described here by two representative time intervals. In general, such coarse representations of the simulated time frame are not sufficient to depict the short-term variability of time-dependent quantities. Mehleri et al. [59] developed a MILP model for SDO optimization of a neighbourhood system integrating DHN with CHP units and distributed photovoltaic (PV) generation. To properly consider the short-term variability of solar radiation, they used a representative day for each month of the year with a temporal resolution of one hour. However, they simplified the network representation by considering the pipelines as direct, straight connections between adjacent buildings, regardless of the actual topology and geographic configuration of the neighbourhood. In addition to DHN, Yang et al. [60] and Sidnell et al. [61] also introduced SDO optimization of an electrical microgrid (EMG), keeping the same simplified approach as in the previous case to model both networks. A more detailed representation of the system topology was provided by Girardin et al. [65] who constrained DHN pipelines to follow only predetermined paths such as roads in a district, thus avoiding impractical connections between nodes. Lerbinger et al. [66] considered a DHN expansion problem with the possibility of connecting some neighbourhoods in a city to the existing DHN, with the goal of integrating a larger share of renewable generation. Again, DHN optimization is based on the actual geography of the system, with city streets as the only available routes for the pipes. Morvaj et al. [67] demonstrated that a "street-following approach" to DHN design provides more reliable solutions than a "green-field approach" that allows all possible connections between buildings while ignoring the actual geography of the system. Note that the street-following approach is applied here only to DHN. Comodi et al. [68] optimized the MES of a university campus in Singapore to find the mix of energy conversion and storage systems and internal network infrastructure needed to fulfil electricity and cooling demand. However, the only internal network considered is the cooling network. Finally, Dos Santos et al. [70] studied the design optimization of the electrical microgrid of a university campus in São Paulo, Brazil, by considering the sizing and placement of distributed generation units and battery energy storage systems, as well as the sizing of the microgrid cables. In this publication, however, the authors considered only the electrical system and not a MES configuration.

1.1. Object, novelty and goal of the work

The gaps emerging from the literature review are associated with excessive simplifications of the SDO problem of a MES, which includes an extremely high number of continuous and binary decision variables. These simplifications are required to make the problem computationally solvable and are listed below:

- The chosen temporal resolution is often too coarse [53–58]. The entire system life cycle is aggregated into a few representative time intervals, and this is not acceptable if short-term variability in input data (energy demand, availability of intermittent renewable sources, prices) is to be taken into account;
- The system topology is often modelled in an oversimplified way according to a "green-field approach" [59–64]. Network lines are considered as direct, straight connections between adjacent buildings, regardless of the path they must follow in the real system. A more proper approach is to plan networks on the basis of the geographical map where the system is located, on which the possible paths that the lines must follow are identified (e.g., "street-following approach" [50]). This avoids unfeasible interconnections;
- In most cases, beside many energy conversion and storage technologies, only the DHN or cooling network is considered [65–69]. Other networks, such as the electrical one, are regarded at most as system constraints and are not optimized in terms of layout and capacity [42,43].

This paper presents a novel optimization method for the SDO of a MES in its entirety: "*DOMES*" (acronym for *Design Of Multi-Energy Systems*). DOMES is able to find the location, type, size, and operation of the energy conversion and storage units that meet the energy demand of end users, together with the topology and capacity of the energy networks delivering to them the useful energy. It overcomes the three above-mentioned gaps, respectively, as follows:

- The multi-year time framework of the optimization problem is represented by typical days (TDs) with hourly resolution that accurately reproduce both the long-term and short-term variability of the time series;
- The energy networks are modelled according to the "street-following approach" in order to generate system layouts that comply with the actual geographical configuration of the system;
- Multiple energy networks can be optimized in combination, potentially, with any kind of energy conversion and storage technology, renewable-based or not, dispatchable or not.

The novelty of this integrated approach is that it comprehensively solves an optimization problem that so far has been only partially addressed in the literature because of the strong simplifications required for computational feasibility. Moreover, DOMES is capable of designing the new MES "from scratch" or performing "retrofit design" of an existing one, where retrofit design refers to the possibility of adding new components to an existing system or new capacity to the components already available [71]. However, other simplifications are still needed in order to find solutions in reasonable computational times. These simplifications must ensure a sufficiently good accuracy of the solution, which may be improvable, but is the only one that can be practically achieved.

The final goal is to develop an optimization tool that can provide decision makers with clear and accurate information on how to properly plan, design, and schedule the operation of a MES in the context of a sustainable energy transition towards a decarbonized economy.

As mentioned above, the combinatorial nature of binary variables in a MILP problem causes the computational requirements to increase exponentially with their number, thus making large-scale problems computationally unsolvable [72]. To overcome this inherent limitation of MILP, DOMES combines two mathematical techniques: time series aggregation [73] and problem decomposition [74]. Note that an SDO model of a MES mainly contains two types of binary decision variables: synthesis variables (existence of a plant or network line), which are

time-independent, and operational variables (e.g., the on/off status of a plant), which are time-dependent. On the one hand, to reduce the temporal dimension of the problem, time-dependent input data, generally available for one year with an hourly resolution, are aggregated into representative TDs using a K-medoids clustering technique [75]. On the other hand, the SDO model is decomposed into two levels by means of an evolutionary algorithm (EA) that isolates the synthesis variables from the rest of the optimization problem. The developed bilevel EA governs the two levels as follows:

- *Upper level: synthesis*. The upper level sets all the binary variables associated with the synthesis problem, i.e., the inclusion/exclusion of a certain plant at a certain node, the inclusion/exclusion of a network line between two nodes. This upper level then provides the lower level with a set of possible combinations of synthesis variables;
- *Lower level: design and operation*. For each combination of synthesis variables provided by the upper level, the lower level optimizes the sizing and operation of the energy conversion and storage plants and network lines included in the system with a MILP approach. This allows many MILP optimizations containing a small number of binary operational variables to be performed in parallel, thereby drastically reducing the computational load of the overall problem.

The developed optimization method introduces some novel features in the context of decomposition techniques for MES optimization. First, the two-level decomposition separates the synthesis problem from the design and operation problem to reduce as much as possible the number of binary variables in the MILP framework at the lower level. In contrast, the common approach in the literature (see, e.g., Casisi et al. [69]) is to separate time-independent variables (synthesis and design) from time-dependent variables (operation). However, design variables are continuous and, with proper linearization, can be optimized in the MILP problem at the lower level along with operation. This speeds up the solving procedure because MILP solvers are faster than meta-heuristic solvers. Second, a strict set of rules is introduced in the EA to minimize inconsistent topological configurations at the upper level, thus reducing the number of infeasible solutions and further decreasing the computational time. Fig. 2 schematically depicts the optimization algorithm of DOMES, which is discussed in detail in Section 2. Note that the EA requires a number of iterations to converge to the optimal solution.

A case study based on a district MES located in Padova, Italy, demonstrates the potential of the proposed method. PV panels, gas-fired CHP internal combustion engines (ICEs), air-water heat pumps (HPs), gas boilers (GBs), thermal energy storage (TES) and electric energy storage (EES) systems are considered along with heating and electrical networks. The goal consists in minimizing the life-cycle cost of the MES to meet the heat and electricity demand of the users, with the possibility of setting an upper limit on CO_2 emissions as a secondary objective.

The rest of the paper is structured as follows. Section 2 describes the proposed method in detail. Sections 3 and 4 present the case study and obtained results, respectively, considering both "design from scratch" and "retrofit design". Section 5 discusses the findings and limitations that have emerged. Finally, Section 6 summarizes the conclusions.

2. Method

This section provides detailed information about the DOMES architecture. Before describing the complete optimization problem and its MILP framework (Section 2.2), general information about the mathematical modelling is given (Section 2.1). Finally, the decomposition of the problem is introduced, and the proposed two-level EA is discussed (Section 2.3).

2.1. General modelling information

The purpose of DOMES is to model the geographic area of the system with satisfactory spatial resolution and to identify the possible locations of buildings, energy conversion and storage units, and network lines. Thus, a MES is considered as a multi-nodal system, where N is the set of nodes in the system. Each node $n \in N$ is described by a pair of coordinates x_n and y_n representing the location of the node "on the map" with respect to a reference point. Nodes represent buildings, places where energy conversion plants can be installed, points of interconnection with external systems (e.g., main electricity and gas grids), and any other type of a relevant point (e.g., road crossings). Allowable connections between nodes define the paths where network lines can be placed. The set N, which contains the required geographic information, is provided as input to the model. Additional input information associated with each node includes the following data.

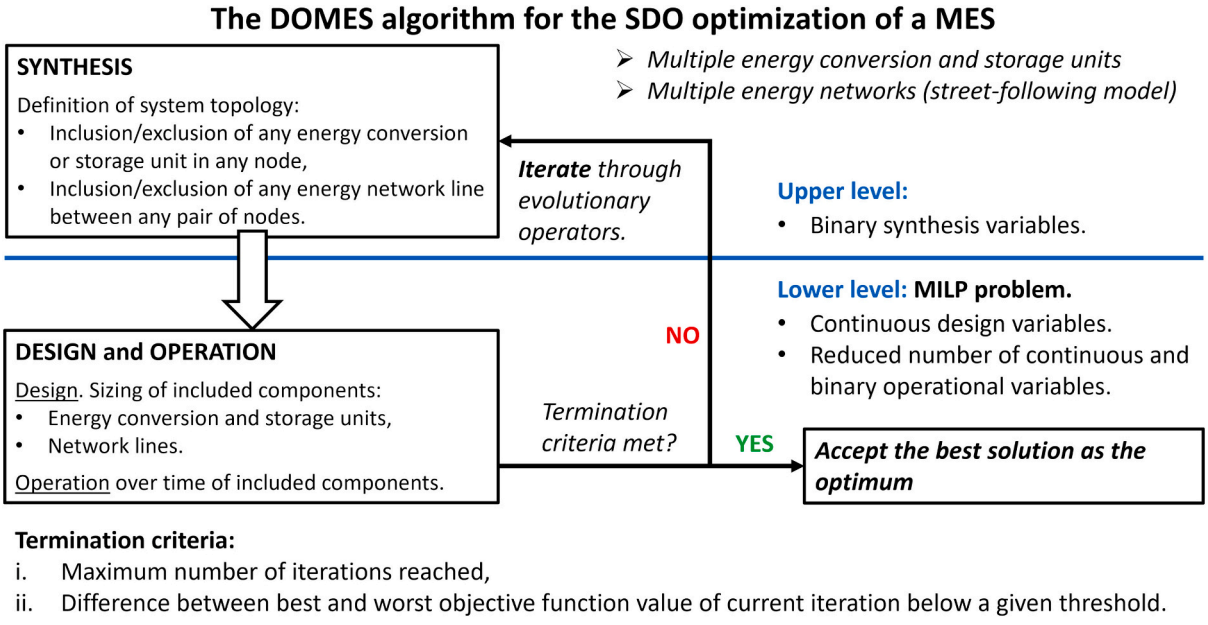

Fig. 2. Structure of the DOMES optimization method.

- The power demand χ_e over time associated with each energy carrier $e \in E$, where E is the set of energy carriers considered (e.g., heat, electricity, natural gas, etc.). Note that only nodes associated with an end user have actual energy demand. The demand is zero for all other nodes.
- Permission to import/export energy carrier $e \in E$ from/to the external systems (e.g., electric or gas grid).
- Dispatchable energy conversion technologies that can be installed (e.g., ICE, GB, HP, gas turbines, etc.), chosen from the set C.
- Non-dispatchable energy conversion technologies that can be installed, chosen from the set R, which mainly includes technologies based on intermittent renewable sources (e.g., PV, wind turbines, etc.).
- Energy storage technologies that can be installed (e.g., batteries, hot water tanks), chosen from the set S.

Other inputs required by the model are technical and economic data associated with energy conversion and storage technologies (off-design maps, operating limits, capital costs, etc.), prices of energy carriers that can be imported/exported from/to external systems, weather and other relevant time series that provide, for instance, resource availability (e.g., solar irradiation).

2.1.1. Time series aggregation

To properly plan a system over its entire life cycle, it is necessary to consider the variability of time-dependent input data over a sufficiently long period with satisfactory temporal resolution. The usual approach in MES modelling is to consider annual time series with an hourly resolution, by using a representative year of the system operation [29]. Accordingly, time dependent data are defined for each hour $t \in T = \{1, 2, \ldots, 24\}$ of each day of the year $d \in D = \{1, 2, \ldots, 365\}$, for a total of 8760 timesteps. However, the computational load of the optimization problem increases at least linearly with the total number of timesteps. Thus, SDO problems may become computationally unsolvable, especially when many binary variables are required.

The proposed method makes use of K-medoids clustering to reduce the total number of timesteps and, in turn, the computational requirements of the problem [75]. K-medoids clustering allows extracting from the set $D = \{1, 2, \ldots, 365\}$ a subset $K \in D$ of TDs representing the entire year. This reduces the temporal dimension of the problem form $T \times D$ to $T \times K$. The number of elements $k \in K$ is an input data of the clustering algorithm and must be chosen as a trade-off between reducing computational load and preserving satisfactory accuracy of the aggregated time series.

The outputs of the clustering algorithm are:

- The set of TDs $K \in D$ and the corresponding aggregated time series of dimension $T \times K$;
- The weight w_k of each TD $k \in K$, i.e., the number of annual days represented by k;
- The map function $g : g(d) = k$ that associates each day of the year d to the TD k representing it.

2.2. Optimization problem

The overall SDO optimization problem is formulated as a MILP problem. This section introduces the decision variables, objective function and constraints.

2.2.1. Decision variables

Decision variables can be grouped into three categories: synthesis, design, and operational. While synthesis and design variables are not time dependent, operational variables depend on time and are therefore defined for each timestep of the problem. Continuous variables are defined in the domain of non-negative real numbers. Binary variables belong to the binary domain $\{0, 1\}$.

All synthesis variables (see Table 1) are binary and indicate the existence (1) or nonexistence (0) of a component. The user can decide about part of the synthesis variables before performing the optimization. This allows (i) to avoid impractical connections between nodes or impractical placement of components and (ii) to declare components that are already available in the system or that must be installed for sure. Note that if a bidirectional flow is allowed in a network, the corresponding decision variables are symmetrical ($\Delta^{net}_{e,n,m} = \Delta^{net}_{e,m,n}$: if node n is connected to node m, the reverse is also true).

All design decision variables (see Table 2) are continuous and indicate the size (rated capacity) of components in terms of power (for energy conversion plants and network lines) or energy (for storage systems).

Operational decision variables (see Table 3) can be either continuous or binary and are defined for each timestep of the problem. Continuous variables include power flows within network lines, power input and output of energy conversion and storage units, power import/export from/to external systems, state of charge (SOC, i.e., energy content) of storage systems and auxiliary variables. Binary variables include the on/off status of dispatchable energy conversion technologies.

2.2.2. Objective function

The objective function set by default is the system life-cycle cost, i.e., the sum of capital and operating costs over the entire lifetime of the plants and networks under consideration. However, any other type of objective function can be implemented, provided the necessary data are available. Eq. (1) defines the objective function in terms of annual levelized investment costs (Γ^{cap}, i.e., capital costs), and annual operating costs (Γ^{oper}).

$$f = \Gamma^{cap} + \Gamma^{oper} \tag{1}$$

Capital costs of components are expressed as linear function of the rated capacity to consider economy-of-scale effects. This linearization is required to keep the problem computationally solvable, and its range of application is limited to a given maximum size for each component. Eq. (2) defines the total capital cost, where τ is the actualization factor calculated according to Eq. (3) (where, in turn, ρ is the interest rate and ι is the expected lifetime in *years*), α is the size-specific investment cost expressed in $€/kW$ for energy conversion technologies, $€/kWh$ for storage technologies and $€/kW/m$ for energy networks, β is the fixed investment cost expressed in $€$ for energy conversion and storage technologies and $€/m$ for energy networks, ν is the relative operation

Table 1
Synthesis decision variables, all binaries.

Variable	Description
$\Delta^{C}_{c,n}$	Existence of the dispatchable energy conversion technology c at node n
$\Delta^{R}_{r,n}$	Existence of the non-dispatchable energy conversion technology r at node n
$\Delta^{S}_{s,n}$	Existence of the energy storage technology s at node n
$\Delta^{exc}_{e,n}$	Permission of node n to import/export the energy carrier e from/to external systems
$\Delta^{net}_{e,n,m}$	Existence of the energy network line associated with the carrier e from node n to node m, $n \neq m$

Table 2
Design decision variables, all continuous.

Variable	Description
$Z^{C}_{c,n}$	Rated capacity of the dispatchable energy conversion technology c at node n
$Z^{R}_{r,n}$	Rated capacity of the non-dispatchable energy conversion technology r at node n
$Z^{S}_{s,n}$	Rated capacity of the energy storage technology s at node n
$Z^{net}_{e,n,m}$	Rated capacity of the energy network line (carrier e) from node n to node m, $n \neq m$

Table 3
Operational decision variables, either binaries or continuous.

Variable	Description	Type
$\pi^{C}_{c,e,n,k,t}$	Power output in terms of energy carrier e of the dispatchable energy conversion technology c at node n during the timestep t of typical day k	continuous
$\mu^{C}_{c,e,n,k,t}$	Power input in terms of energy carrier e of the dispatchable energy conversion technology c at node n during the timestep t of typical day k	continuous
$\delta^{C}_{c,n,k,t}$	On/off state of the dispatchable energy conversion technology c at node n during the timestep t of typical day k	binary
$\vartheta^{C}_{c,n,k,t}$	Auxiliary variable associated with the dispatchable energy conversion technology c at node n during the timestep t of typical day k	continuous
$\pi^{S}_{s,e,n,k,t}$	Discharge power in terms of energy carrier e of the energy storage technology s at node n during the timestep t of typical day k	continuous
$\mu^{S}_{s,e,n,k,t}$	Charge power in terms of energy carrier e of the energy storage technology s at node n during the timestep t of typical day k	continuous
$\xi^{intra}_{s,e,n,k,t}$	Intra-day state of charge in terms of energy carrier e of the energy storage technology s at node n during the timestep t of typical day k	continuous
$\xi^{inter}_{s,e,n,d}$	Inter-day state of charge in terms of energy carrier e of the energy storage technology s at node n during the day of the year d	continuous
$\xi^{intra,max}_{s,e,n,k}$	Maximum intra-day state of charge in terms of energy carrier e of the energy storage technology s at node n during typical day k (auxiliary variable)	continuous
$\xi^{intra,min}_{s,e,n,k}$	Minimum intra-day state of charge in terms of energy carrier e of the energy storage technology s at node n during typical day k (auxiliary variable)	continuous
$\psi^{imp}_{e,n,k,t}$	Power imported from external systems in terms of energy carrier e at node n during the timestep t of typical day k	continuous
$\psi^{exp}_{e,n,k,t}$	Power exported to external systems in terms of energy carrier e at node n during the timestep t of typical day k	continuous
$\varphi^{net}_{e,n,m,k,t}$	Power flow in the network line (carrier e) from node n to node m, $n \neq m$, during the timestep t of typical day k	continuous

and maintenance cost, and $l(n,m)$ is the distance from node n to node m expressed in m and calculated according to Eq. (4).

$$\begin{aligned} I^{cap} = \sum_{n\in N}\Bigg\{ & \sum_{c\in C}\left[\tau^{C}_{c}\left(\alpha^{C}_{c}Z^{C}_{c,n}+\beta^{C}_{c}\Delta^{C}_{c,n}\right)\left(1+\frac{\nu^{C}_{c}}{\tau^{C}_{c}}\right)\right] \\ & + \sum_{r\in R}\left[\tau^{R}_{r}\left(\alpha^{R}_{r}Z^{R}_{r,n}+\beta^{R}_{r}\Delta^{R}_{r,n}\right)\left(1+\frac{\nu^{R}_{r}}{\tau^{R}_{r}}\right)\right] \\ & + \sum_{s\in S}\left[\tau^{S}_{s}\left(\alpha^{S}_{s}Z^{S}_{s,n}+\beta^{S}_{s}\Delta^{S}_{s,n}\right)\left(1+\frac{\nu^{S}_{s}}{\tau^{S}_{s}}\right)\right] \\ & + \sum_{e\in E}\sum_{m\in N,m\neq n}\left[\tau^{net}_{e}\left(\alpha^{net}_{e}Z^{net}_{e,n,m}+\beta^{net}_{e}\Delta^{net}_{e,n,m}\right)\left(1+\frac{\nu^{net}_{e}}{\tau^{net}_{e}}\right)l(n,m)\right]\Bigg\} \end{aligned} \tag{2}$$

$$\tau^{C(R,S,net)}_{c(r,s,e)} = \frac{\rho(1+\rho)^{l^{C(R,S,net)}_{c(r,s,e)}}}{(1+\rho)^{l^{C(R,S,net)}_{c(r,s,e)}}-1} \tag{3}$$

$$l(n,m) = l(m,n) = \sqrt{(x_n-x_m)^2+(y_n-y_m)^2} \tag{4}$$

Eq. (5) defines the annual operating costs considering expenses for imported (superscript *imp*) energy and revenues for exported (superscript *exp*) energy, where γ_e is the specific cost/price of carrier e in $€/kWh$, and h is the considered timestep size, which is equal to one hour.

$$I^{oper} = \sum_{n\in N}\sum_{e\in E}\sum_{k\in K} w_k \sum_{t\in T} h\left(\gamma^{imp}_{e,k,t}\psi^{imp}_{e,n,k,t} - \gamma^{exp}_{e,k,t}\psi^{exp}_{e,n,k,t}\right) \tag{5}$$

2.2.3. Constraints

The constraints of the problem include the power balances of each energy carrier at each node and the off-design maps of the components, which have been linearized according to MILP. An additional constraint can be imposed on the maximum amount of CO_2 produced directly and indirectly by the system.

Power balances

Eq. (6) defines power balances, where λ^{net} is a network-specific loss factor in m^{-1}, and $\sigma^{net}(*)$ is a correction factor as a function of generic (time-dependent) input data * (e.g., DHN losses may vary as the ground temperature changes).

$$\begin{aligned} \psi^{imp}_{e,n,k,t} + \sum_{c\in C}\pi^{C}_{c,e,n,k,t} + \sum_{r\in R}\pi^{R}_{r,e,n,k,t} + \sum_{s\in S}\pi^{S}_{s,e,n,k,t} + \sum_{m\in n,m\neq n}\varphi^{net}_{e,m,n,k,t}\left[1-\lambda^{net}_{e}l(nm)\sigma^{net}_{e,k,t}(*)\right] = \chi_{e,n,k,t} + \psi^{exp}_{e,n,k,t} + \sum_{c\in C}\mu^{C}_{c,e,n,k,t} + \sum_{s\in S}\mu^{S}_{s,e,n,k,t} \\ + \sum_{m\in n,m\neq n}\varphi^{net}_{e,n,m,k,t} \;\forall\, e\in E, n\in N, k\in K, t\in T \end{aligned} \tag{6}$$

The sum of all power flows of a certain carrier entering a node must equal the sum of all power flows of the same carrier exiting that node. Note that the power flow entering a node through a network line is equal to the power flow exiting the other extreme node of that line reduced by the losses.

Non-dispatchable energy conversion technologies

The output power of the non-dispatchable energy conversion technology r in terms of carrier e ($\pi^{R}_{r,e}$) depends on its rated capacity and, possibly, some (time-dependent) input data, as given in Eq. (7), where $\sigma^{R}(*)$ is a correction factor that depends only on input data (e.g., it represents the influence of solar irradiance on the electrical output power of a PV module).

$$\pi^{R}_{r,e,n,k,t} = Z^{R}_{r,n}\sigma^{R}_{r,e,k,t}(*)\;\forall\, n\in N, k\in K, t\in T \tag{7}$$

Moreover, the rated capacity is upper bounded by the maximum value that it can take, $Z^{R,max}$, as given in Eq. (8).

$$Z^{R}_{r,n} \leq Z^{R,max}_{r,n}\Delta^{R}_{r,n}\;\forall\, n\in N \tag{8}$$

The following considerations hold true also for dispatchable conversion and storage technologies:

- If $Z^{R(C,S),max}_{r(c,s)}$ is unknown, it can be set to a "large enough" value;
- The output power is always zero if the technology is excluded ($\Delta^{R(C,S)}_{r(c,s),n} = 0$);
- $\sigma^{R(C,S)}_{r(c,s),e}(*) = 0$ if carrier e does not concern the considered technology.

Dispatchable energy conversion technologies

The output power of the dispatchable energy conversion technology c in terms of carrier e depends on a linear combination of the power inputs of the considered carriers as given in Eq. (9), where $\eta^{C}_{c,e}$ and $\upsilon^{C}_{c,e}$ are constant coefficients that linearize the off-design performance, and $\sigma^{C}(*)$ is a correction factor that depends only on input data (e.g., it represents the influence of ambient temperature on the performance of a gas turbine).

$$\pi^{C}_{c,e,n,k,t} = \sigma^{C}_{c,e,k,t}(*)\sum_{e\in E}\left(\eta^{C}_{c,e}\mu^{C}_{c,e,n,k,t} + v^{C}_{c,e}\delta^{C}_{c,n,k,t}\right) \forall\, n\in N, k\in K, t\in T \quad (9)$$

Note that most technologies have a single input energy carrier. Thus, the correction factor $\sigma^{C}_{c,e}(*)$ is set equal to zero for all carriers except the input one. Moreover, the output power is upper and lower bounded according to the rated capacity and the relative minimum load o^{C}_{c}, as shown in Eqs. (10)–(13), which make use of the auxiliary variable ϑ^{C}_{c} to avoid nonlinear constraints [76].

$$Z^{C}_{c,n} \le Z^{C,max}_{c,n}\Delta^{C}_{c,n} \;\forall\, n\in N \quad (10)$$

$$\vartheta^{C}_{c,n,k,t} \le \delta^{C}_{c,n,k,t}Z^{C,max}_{c,n} \;\forall\, n\in N, k\in K, t\in T \quad (11)$$

$$Z^{C}_{c,n} - \vartheta^{C}_{c,n,k,t} \le \left(1-\delta^{C}_{c,n,k,t}\right)Z^{C,max}_{c,n} \;\forall\, n\in N, k\in K, t\in T \quad (12)$$

$$o^{C}_{c}\vartheta^{C}_{c,n,k,t} \le \pi^{C}_{c,e,n,k,t} \le \vartheta^{C}_{c,n,k,t} \forall n\in N, k\in K, t\in T \quad (13)$$

Note that if $\Delta^{C}_{c,n} = 0$, the power output is zero for all timesteps, whereas if $\delta^{C}_{c,n,k,t} = 0$, the power output is zero only during timestep t of TD k ($\vartheta^{C}_{c,n,k,t} = 0$). Otherwise, if both $\Delta^{C}_{c,n} = 1$ and $\delta^{C}_{c,n,k,t} = 1$, the output power is upper bounded by the rated capacity ($\vartheta^{C}_{c,n,k,t} = Z^{C}_{c,n}$) and lower bounded by the minimum load ($o^{C}_{c}Z^{C}_{c,n}$).

Energy storage technologies

Energy storage technologies are modelled according to Kotzur et al. [77] in order to allow both daily (intra-day) and seasonal (inter-day) storage. Furthermore, a storage technology s is assumed to have only one input and one output of the same carrier e.

Eq. (14) shows the upper and lower bounds of the storage capacity, while Eqs. (15) and (16) limit the charge and discharge power, respectively, according to the capacity-relative coefficients $o^{S,char}_{s}$ and $o^{S,disc}_{s}$ in kW/kWh.

$$Z^{S}_{s,n} \le Z^{S,max}_{s,n}\Delta^{S}_{s,n} \forall n\in N \quad (14)$$

$$\mu^{S}_{s,e,n,k,t} \le o^{S,char}_{s}Z^{S}_{s,n} \forall n\in N, k\in K, t\in T \quad (15)$$

$$\pi^{S}_{s,e,n,k,t} \le o^{S,disc}_{s}Z^{S}_{s,n} \forall\, n\in N, k\in K, t\in T \quad (16)$$

The SOC is composed of two terms, the intra-day SOC ($\xi^{intra}_{s,e}$) and the inter-day SOC ($\xi^{inter}_{s,e}$). The first is defined for each timestep t of each TD k, whereas the latter is defined for each day of the year d.

Eq. (17) reports the dynamic energy balance of the intra-day SOC, which is assumed to be zero at the beginning of the day, as in Eq. (18), where $\lambda^{S}_{s,e}$ is the SOC-relative coefficient of self-discharge losses, $\sigma^{S}_{s,e}$ is a correction factor that depends only on input data (e.g., self-discharge of TES may depend on ambient temperature), $\eta^{S,char}_{s,e}$ is the charging efficiency, and $\eta^{S,disc}_{s,e}$ is the discharging efficiency.

$$\xi^{intra}_{s,e,n,k,t+1} = \xi^{intra}_{s,e,n,k,t}\left[1-\lambda^{S}_{s,e}\sigma^{S}_{s,e,k,t}(*)\right] + \eta^{S,char}_{s,e}\mu^{S}_{s,e,n,k,t}h - \frac{\pi^{S}_{s,e,n,k,t}h}{\eta^{S,disc}_{s,e}} \;\forall\, n\in N, k\in K, t\in T \quad (17)$$

$$\xi^{intra}_{s,e,n,k,t=1} = 0 \;\forall\, n\in N, k\in K \quad (18)$$

The intra-day SOC is bounded by two auxiliary variables ($\xi^{intra,min}_{s,e}$ and $\xi^{intra,max}_{s,e}$), as Eq. (19) shows.

$$\xi^{intra,min}_{s,e,n,k} \le \xi^{intra}_{s,e,n,k,t} \le \xi^{intra,max}_{s,e,n,k} \;\forall\, n\in N, k\in K, t\in T \quad (19)$$

Eq. (20) gives the dynamic energy balance of the inter-day SOC, which is constrained to assume the same value during the first and last day of the year, as Eq. (21) shows.

$$\xi^{inter}_{s,e,n,d+1} = \xi^{inter}_{s,e,n,d}\left[1-\lambda^{S}_{s,e}\sigma^{S}_{s,e,d}(*)\right]^{24} + \xi^{intra}_{s,e,n,k=g(d),t=24} \;\forall\, n\in N, d\in D \quad (20)$$

$$\xi^{inter}_{s,e,n,d=1} = \xi^{inter}_{s,e,n,d=365} \;\forall\, n\in N \quad (21)$$

Thus, the inter-day SOC associated with a day of the year ($d+1$) is given by the sum of the inter-day SOC of the previous day (d) net of self-discharge losses and the residual intra-day SOC at the end of the typical day (k) representing it. Eqs. (22) and (23) define the upper and lower bounds of the overall SOC, respectively, which is the sum of the inter-day and intra-day SOC.

$$\xi^{inter}_{s,e,n,d} + \xi^{intra,max}_{s,e,n,k=g(d)} \le Z^{S}_{s,n} \;\forall\, n\in N, d\in D \quad (22)$$

$$\xi^{inter}_{s,e,n,d}\left[1-\lambda^{S}_{s,e}\sigma^{S}_{s,e,d}(*)\right]^{24} + \xi^{intra,min}_{s,e,n,k=g(d)} \ge 0 \;\forall\, n\in N, d\in D \quad (23)$$

Import and export of energy carriers

Power import/export of carrier e at node n from/to external systems is allowed only if the binary variable $\Delta^{exc}_{e,n}$ is set to 1, as reported in Eqs. (24) (import) and (25) (export), where M is a "large enough" value.

$$\psi^{imp}_{e,n,k,t} \le \Delta^{exc}_{e,n}M \;\forall\, k\in K, t\in T \quad (24)$$

$$\psi^{exp}_{e,n,k,t} \le \Delta^{exc}_{e,n}M \;\forall\, k\in K, t\in T \quad (25)$$

Energy networks

The capacity of the energy network line transporting the carrier e from node n to node m (with $n\neq m$) is upper bounded by a "big-M constraint", where M is a "large enough" value, as given in Eq. (26).

$$Z^{net}_{e,n,m} \le \Delta^{net}_{e,n,m}M \quad (26)$$

If bidirectional flow is allowed, the line capacity is the same in both directions, as given in Eq. (27); otherwise, the flow is only allowed in one direction, as reported in Eq. (28).

$$Z^{net}_{e,n,m} = Z^{net}_{e,m,n} \quad (27)$$

or

$$\Delta^{net}_{e,n,m} + \Delta^{net}_{e,m,n} \le 1 \quad (28)$$

Eq. (29) imposes the upper bound on the power flow in the network line.

$$\varphi^{net}_{e,n,m,k,t} \le Z^{net}_{e,n,m} \;\forall\, k\in K, t\in T \quad (29)$$

Limit on CO_2 emissions and epsilon-constrained multi-objective optimization

The carbon emissions attributable to the system operation are given by Eq. (30) as a function of the imported and exported energy carriers, where ζ is a specific emission factor in kg/kWh.

$$\Phi = \sum_{n\in N}\sum_{e\in E}\sum_{k\in K}w_{k}\sum_{t\in T}h\left(\zeta^{imp}_{e,k,t}\psi^{imp}_{e,n,k,t} - \zeta^{exp}_{e,k,t}\psi^{exp}_{e,n,k,t}\right) \quad (30)$$

Carbon emissions represent direct and indirect production of CO_2. Direct production is associated, for instance, with natural gas imported and subsequently burned in gas engines/boilers. Indirect production is associated, for instance, with the carbon intensity of imported electricity. Emission factors are generally time-dependent and may differ between imported and exported carriers, which usually reduces the CO_2 emissions attributable to the system.

Eq. (31) allows an upper limit to be imposed on CO_2 emissions, where ε is a dimensionless coefficient defined in the range from 0 to 1, and Φ^{0} represents the CO_2 emissions produced if no upper limit is considered.

$$\Phi \le \varepsilon\Phi^{0} \quad (31)$$

By decreasing ε successively from 1 towards 0, it is possible to

perform a so-called "epsilon-constrained" multi-objective optimization [78], thus obtaining as the solution to the problem the Pareto front having life-cycle cost and CO_2 emissions as conflicting objectives.

2.3. Decomposition of the problem by a two-level evolutionary algorithm

To isolate the synthesis decision variables (all binary) from the design and operation decision variables (binary or continuous), DOMES decomposes the full problem into two parts. As introduced in Fig. 2, a two-level EA allows the synthesis variables to be set in the upper level and sent to the lower level, which solves the design and operation problem according to the objective function. EAs are population-based, iterative algorithms. Thus, the upper level defines many combinations of synthesis variables at each iteration, and an equal number of design and operation problems are solved at the lower level by a MILP algorithm. A series of iterations is required to achieve convergence to the optimal solution. This section explains the reasons for choosing the two-level architecture and describes how the EA is structured and solved.

2.3.1. Choice of the two-level architecture

Since the computational complexity of a MILP problem grows exponentially as the number of binary variables increases, the computational load of the lower-level problems is drastically smaller than that of the full problem (in addition, the number of operational binary variables is also reduced due to time series aggregation). Moreover, since the different lower-level problems are independent of each other, they can be solved in parallel, thus further reducing the computational load. As a result, decomposition can reduce the computational time required to solve the SDO optimization of a MES by orders of magnitude, as demonstrated by Casisi et al. [69]. The drawback of this approach is that the meta-heuristic nature of EAs does not provide "internal" mathematical proof that the optimal solution found corresponds to the global optimum [79]. Thus, an "external" procedure is needed to evaluate the "quality" of the obtained solution. Considering the optimization method proposed here, one possibility is to solve the SDO problem of the MES entirely by MILP, thus avoiding decomposition, then comparing the solution obtained with that provided by the two-level EA. In fact, MILP is convex and guarantees finding the global optimum. Therefore, if the result of the EA is sufficiently close to that of MILP, it can be said that the EA has found the global optimum as well. However, especially for large-scale problems, it is rarely possible to solve the SDO optimization entirely by MILP in a reasonable time. To overcome this problem, an alternative validation procedure is presented in Section 5.2.

2.3.2. General concepts and definitions

An "individual" i of the proposed two-level EA is defined as a mathematical object containing all the synthesis decision variables, to which a value is assigned in the upper level. Thus, an individual is associated with a specific system topology. The optimal value of the objective function obtained in the lower level by solving the design and operation MILP problem for that topology is the "fitness value" q of that individual i.

A "generation" is a set I of individuals belonging to the same iteration j. The "parent generation" (I^{par}) refers to a starting generation from which a new generation, the "offspring generation" (I^{off}), can be obtained through proper evolutionary operators. The set of a parent generation and the corresponding offspring generation is called a "population" ($P = I^{par} \cup I^{off}$).

There are three kinds of evolutionary operators: "crossover", "mutation" and "selection" (note that the application of crossover and

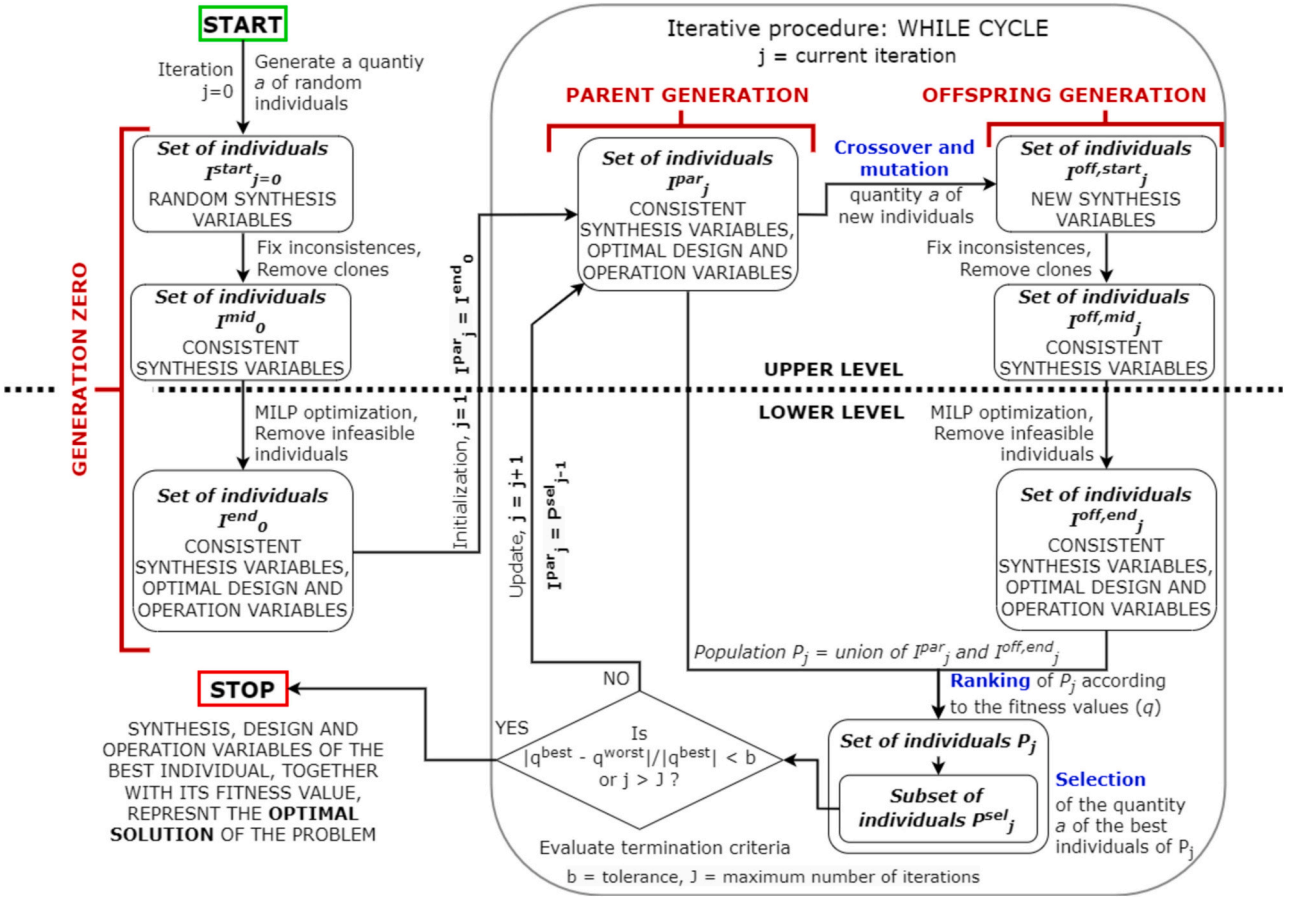

Fig. 3. Flowchart of the two-level EA embedded in DOMES.

mutation operators is limited to the current synthesis decision variables, thus excluding those fixed in advance by the user).

- Crossover combines two "parent individuals" to obtain an "offspring individual". For each synthesis (binary) variable, equal corresponding values in the two parent individuals (1-1 or 0-0) result in the same value in the offspring individual as well (1 or 0, respectively). Different initial values (1-0 or 0-1) cause the corresponding value of the offspring individual to be chosen between 1 and 0 with a 50 % probability.
- Mutation randomly alters the synthesis variables of an individual. Each binary variable has a certain probability (5 % in this case) of changing value.
- Selection groups the best (fittest) individuals in a population based on their fitness values.

2.3.3. Structure of the algorithm and solving procedure

Fig. 3 depicts the flowchart of the two-level EA, which is described below.

In the upper level of EA, the initial generation (generation zero, $j = 0$) is populated with a set $I_{j=0}^{start}$ containing a quantity a of randomly created individuals (i.e., for each individual $i \in I_{j=0}^{start}$ a random binary variable is assigned to each synthesis decision variable). These random data structures are called "starting representations" (SRs) of individuals and may contain inconsistencies that would result in infeasible or nonoptimal solutions. A rigorous set of rules is introduced to fix inconsistencies and, in turn, reduce the number of meaningless individuals, thus speeding up the EA. Specifically, four rules are applied in the following order.

(1) Detect whether a network line is not connected to any end user, import/export node, or energy conversion/ storage plant. If so, remove that network line and iterate if another line has the same inconsistency.
(2) Detect whether an isolated part of a network does not include at least one end user and any other end user, import/export node, or conversion/storage plant. If so, remove that isolated part of the network and iterate to fix all similar inconsistencies.
(3) Detect whether an end user is isolated without the availability of energy conversion plants to meet its demand. In this case, no general solution is available. Only case-specific solutions can be applied (e.g., adding a GB to an isolated end user with heat demand). If not even a case-specific solution is available, the inconsistency remains.
(4) Detect whether an energy conversion or storage plant is isolated. If so, remove that energy conversion or storage plant and iterate until there are no more isolated plants.

The data structure of an individual after checking and possibly fixing the inconsistencies is called the "intermediate representation" (IR). IRs are checked again to identify clones (i.e., individuals with the same IR), which are removed from the set $I_{j=0}^{start}$ to obtain the new set $I_{j=0}^{mid}$.

The IRs of the set $I_{j=0}^{mid}$ are then provided as input to the lower-level design and operation problem, which, for each individual $i \in I_{j=0}^{mid}$, finds all the design and operational decision variables and calculates the corresponding fitness value q. Individuals with infeasible solutions (due, for example, to residual inconsistencies) are removed from $I_{j=0}^{mid}$ to obtain the new set $I_{j=0}^{end}$. The data structure of individuals $i \in I_{j=0}^{end}$, which now also contains the optimal value of all design and operational decision variables along with the associated fitness value q, is called the "optimal representation" (OR).

Individuals of $I_{j=0}^{end}$ populate the parent generation of the first iteration $I_{j=1}^{par}$ with their SRs, IRs, and ORs. At this point the iterative cycle of the two-level EA begins and follows the steps given below:

(1) A quantity a of pairs of individuals is randomly selected from the set I_j^{par}. For each pair, the crossover operator is applied to the SRs to obtain a new individual. Then, the mutation operator is applied to the new individual. Thus, a quantity a of new individuals with their SRs is obtained. These populate the offspring generation in the upper level of the current iteration j, thus defining the new set $I_j^{off,start}$;
(2) Each individual $i \in I_j^{off,start}$ is checked for inconsistencies that may arise due to the random nature of the crossover and mutation operators. The inconsistencies are eventually fixed according to the above-mentioned set of rules, resulting in the IRs. Then $I_j^{off,start}$ is checked to find any clones, which are removed, thus obtaining the new set $I_j^{off,mid}$;
(3) The IRs of individuals from $I_j^{off,mid}$ are sent to the lower level, where the design and operation problem is solved for each individual $i \in I_j^{off,mid}$, thus obtaining the optimal value of all design and operation decision variables along with the associated fitness value q. Individuals associated with infeasible solutions are removed from $I_j^{off,mid}$, thus obtaining the new set $I_j^{off,end}$ including the new ORs;
(4) The population $P_j = I_j^{off,end} \cup I_j^{par}$ is generated. Individuals in P_j are then ranked from best to worst according to their fitness values;
(5) The selection operator extracts the first (best) a individuals of P_j, thus obtaining the new set $P_j^{sel} \in P_j$;
(6) The termination criteria are evaluated. If the relative difference (gap) between the fitness value of the best (first) individual of P_j^{sel}, $q\left(i^{best} \in P_j^{sel}\right)$, and that of the worst (last) individual, $q\left(i^{worst} \in P_j^{sel}\right)$, is less than a certain threshold b, or if the number of iterations j reaches the maximum allowed number J, then the algorithm stops and the values of the synthesis, design and operational decision variables of i^{best}, together with its fitness value, represent the optimal solution to the problem. Otherwise, the iteration counter is updated ($j = j + 1$) and the individuals of P_j^{sel} populate the new parent generation I_j^{par} with their SRs, IRs and ORs. Then, the algorithm returns to step 1.

The number of individuals a populating the parent generations and the termination tolerance b are critical parameters to choose. The larger a, the wider the search space of the optimization problem and the lower the chance of obtaining a local optimum as the final results, but also the higher the computational requirements. The lower b, the higher the probability of finding the global optimum with good accuracy while avoiding suboptimal solutions, but, again, the higher the computational time. It is also possible to set a maximum number of iterations J to stop the EA in case the termination tolerance is not reached in a reasonable time. However, the farther the gap of the last iteration from the termination tolerance b, the lower the probability of finding the global optimum.

3. Case study

Fig. 4 shows the geographic layout of the case study considered here, which represents a district in the city of Padova, Italy. Meteorological data of solar irradiation and ambient temperature are available for one year with hourly resolution [80]. The district is modelled as a multi-nodal system with a total of 36 nodes. The possible connections between pairs of nodes define the allowed path for the network lines. The

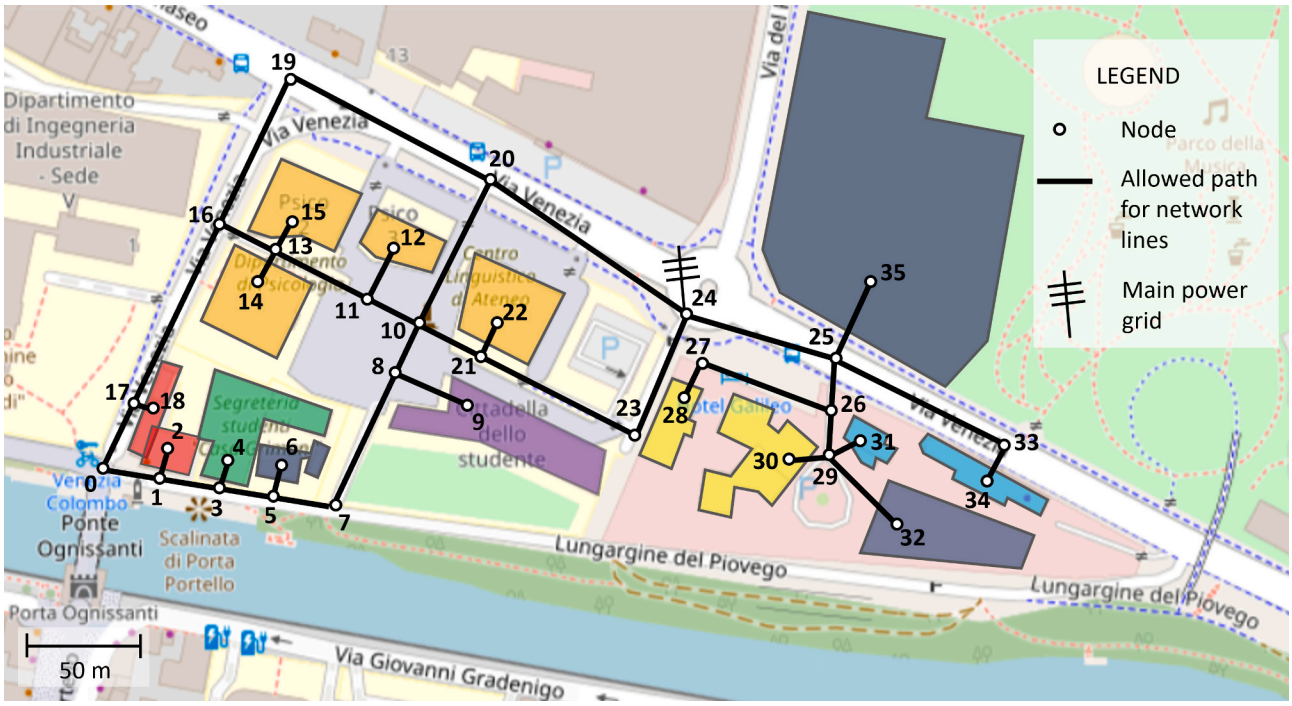

Fig. 4. Layout of the considered MES.

Table 4
End users of the considered MES with their energy demand.

Node	Type of building	Annual electrical demand, *MWh*	Electrical demand peak, *kW*	Annual heat demand, *MWh*	Heat demand peak, *kW*
2	Restaurant	91.3	20	49.4	30
4	Offices	112.8	45	24.2	70
9	Residential	574.5	160	429.0	350
12	University	192.4	75	66.6	125
14	University	230.9	90	79.9	150
15	University	218.1	85	74.6	140
18	Restaurant	68.5	15	36.2	22
22	University	269.4	105	95.9	180
28	Hotel	213.9	50	235.7	110
30	Hotel	427.8	100	471.4	220
31	Shop	52.9	12	21.0	18
34	Shop	132.2	30	49.0	42

Table 5
Energy hubs of the considered MES and connections with external systems.

Node	Type of node	Allowed technologies (maximum capacity), Energy carriers that can be exchanged
6	Energy hub	PV($50kW_p$), ICE($200kW_{el}$), GB($2MW_{th}$), HP($300kW_{th}$), TES ($300kWh$), EES($50kWh$)
24	Connection	Electricity import/export from/to the main power grid
32	Energy hub	ICE($1MW_{el}$), GB($2MW_{th}$), HP($1MW_{th}$), TES($1MWh$)
35	Energy hub	PV($2MW_p$), ICE($1MW_{el}$), GB($2MW_{th}$), HP($1.5MW_{th}$), TES ($1.5MWh$), EES($500kWh$)

system includes 12 public, commercial and residential end users, shown in Table 4 with their heat and electricity demands (available for one year with hourly resolution). This study considers PV, GB, CHP ICE, air-water HP, EES and TES as energy conversion and storage units that can be installed to meet the user demands, and DHN and EMG as networks. The EMG is assumed to operate at low voltage (400 V), while the DHN is assumed to operate with pressurized hot water with constant supply and return temperatures of 70 °C and 40 °C, respectively. In addition to

Table 6
Linearized investment costs and lifetime of the considered technologies and carriers [81–83].

Technology	Size-specific cost (α)	Fixed cost (β)	Lifetime (ι), *years*
PV	$1250€/kW_p$	0	20
ICE	$1740€/kW_{el}$	32.0k€	20
GB	$65€/kW_{th}$	1.6k€	20
HP	$117€/kW_{th}$	2.1k€	20
TES	$244€/kWh$	1.0k€	20
EES	$880€/kWh$	3.5k€	20
EMG	$10€/kW/km$	$34€/m$	40
DHN	$200€/kW/km$	$103€/m$	40

electricity and heat, natural gas is considered as an energy carrier. However, the gas network has not been modelled, assuming that it is already available. Thus, energy conversion technologies that require natural gas are assumed to import it directly from the external gas grid. The local EMG can be connected to the external power grid at node 24. In contrast, the DHN remains isolated in the district. Energy conversion and storage units, with the exception of ICEs, can be installed directly at the end-user-building level. Alternatively, three energy hubs have been identified to install larger plants, including ICEs, according to Table 5. Table 6 shows the investment cost coefficients of the considered plants and networks and their expected lifetimes. Table 7, Table 8 and Table 9 report the operating parameters of energy conversion technologies, storage technologies and networks, respectively. Finally, Table 10 reports the specific costs/prices and emission factors of energy carriers, assumed as constant values throughout the year. A more detailed analysis of the considered components can be found in Refs. [71, 81].

Two types of problems have been considered and solved to show the potential of DOMES in optimizing the SDO of a MES:

- *Design from scratch* (Section 4.1). Starting with a blank system, the goal is to find the location, type, size, and operation of energy conversion and storage units and the network topology that minimize the life cycle cost of meeting the demand of end users;
- *Retrofit design* (Section 4.2). A set of energy conversion and storage plants and network lines are already available in the system. The goal

Table 7
Operational parameters of the considered energy conversion technologies [81–83].

Parameter		PV	ICE	GB	HP
Type		Non-dispatchable	Dispatchable	Dispatchable	Dispatchable
Input carrier		–	Natural gas	Natural gas	Electricity
Input time series affecting the operation (*)		Solar irradiation H, kW/m^2	–	–	Ambient temperature Θ, K
Minimum load (o)		–	0.7	0	0.5
First output	Carrier (e)	Electricity	Electricity	Heat	Heat
	Flow-specific output coefficient (η_e)	–	0.41	0.9	0.56
	Fixed output coefficient (υ_e), kW	–	−4.55	0	−2.10
	Correction factor (σ_e)	$H_{k,t}/H^{std}$ [1]	1	1	$(\Theta^s - \Theta_{k,t})/\Theta^s$ [2]
Second output	Carrier (e)	–	Heat	–	–
	Flow-specific output coefficient (η_e)	–	0.51	–	–
	Fixed output coefficient (υ_e), kW	–	−7.29	–	–
	Correction factor (σ_e)	0	1	0	0

[1] H^{std}: standard solar irradiation at peak conditions (1000 W/m^2).
[2] Θ^s: supply temperature (343.15 K).

Table 8
Operational parameters of the considered energy storage technologies [81–83].

Parameter	TES	EES
Input and output carrier (e)	Heat	Electricity
Input time series affecting the operation (*)	–	–
Charging capacity (o^{char}), kW/kWh	1	1
Discharging capacity (o^{disc}), kW/kWh	1	1
Charging efficiency (η^{char})	1	0.95
Discharging efficiency (η^{disc})	1	0.95
Relative self-discharge losses (λ)	0.04	0
Correction factor (σ_e)	1	1

Table 9
Operational parameters of the considered energy networks [81–83].

Parameter	EMG	DHN
Carrier (e)	Electricity	Heat
Input time series affecting the operation (*)	–	–
Relative loss-factor (λ), $1/m$	5.4×10^{-5}	5.0×10^{-6}
Correction factor (σ_e)	1	1

Table 10
Specific costs/prices and emission factors of the considered energy carriers [81,84,85].

Carrier	Import cost (γ^{imp}), €/MWh	Export price (γ^{exp}), €/MWh	Import emission factor (ζ^{imp}), kg/MWh	Export emission factor (ζ^{exp}), kg/MWh
Electricity	234	50	356	0
Natural gas	98	*n.d.*	197	*n.d.*
Heat	*n.d.*[1]	*n.d.*	*n.d.*	*n.d.*

[1] *n.d.* = not defined.

is to improve the economic and environmental performance of the initial system configuration by installing new components and/or adding capacity to existing ones.

Annual time series of energy demand and weather data are aggregated into 10 typical days that include the two days of the year with the maximum peak of electricity and heat demand, respectively. Considering EA, the number of individuals per generation (a) is set to 100, the termination tolerance (b) to 10^{-3} and the maximum number of iterations to 100. These assumptions are discussed in Section 5.

4. Results

The DOMES framework is developed in Python and uses Gurobi as MILP optimizer. Optimizations have been performed by a machine with an Intel(R) Core(TM) i9-12900K 3.20 GHz processor and 64 Gb RAM.

4.1. Design from scratch

The design from scratch has been solved in about 6 h, reaching termination tolerance in 50 iterations.

Fig. 5 shows the optimal layout of EMG and DHN obtained by design from scratch. Both networks are radial and not meshed. This is due to the effects of economies of scale, which favor the installation of fewer lines of higher capacity to reduce the investment cost. The EMG connects all end users with the energy hubs at nodes 6 and 35 and with the main power grid at node 24, thus highlighting that working in island mode is not cost-effective for the system. The DHN also connects all end users with the energy hubs at nodes 6 and 35, with the exceptions of the users located at nodes 12, 14, and 15, which must therefore provide for their heat demand individually.

Fig. 6 shows how the capacity of the networks is distributed among the EMG and DHN lines and how the capacity of the installed energy conversion and storage units is distributed among the nodes. The energy hub at node 35 includes the largest PV plant in the system (613 kW_p) along with an ICE of 174 kW rated electrical capacity, a HP of 183 kW rated thermal capacity, and a TES of 231 kWh rated capacity. Smaller PV systems are distributed among all end-user buildings. The energy hub at node 6 includes a GB of 291 kW rated thermal power, a HP of 196 kW rated thermal power, and a TES of *37* kWh rated capacity. The end users not connected to the DHN install independently GB, HP, and TES to meet their heat demand, while the users connected to the DHN draw the required heat entirely from the network. The largest DHN pipelines (up to 511 kW capacity) are those near the energy hubs because they take over the heat supply for the entire network. In fact, the DHN has a "tree" shape, with heat streams flowing only from the hubs (roots) to the users (leaves). Thus, end users are not allowed to inject thermal energy into the network but only to withdraw it. In contrast, the energy flows within the EMG are bidirectional. In this case, the largest lines (up to 516 kW capacity) are those near node 24, i.e., the point of connection to the main power grid, which takes over the entire import and export of electricity for the system. Note that no EES is installed because it is not cost-effective due to its relatively high investment cost. The coupling of PV, HP and TES turns out to provide sufficient flexibility at lower costs than installing EES.

The levelized annual cost of the MES is 509.8 $k€$, and the annual CO_2 emissions are 618.6 t. These results can be compared with a reference case in which users meet the entire heat demand with gas-fired boilers

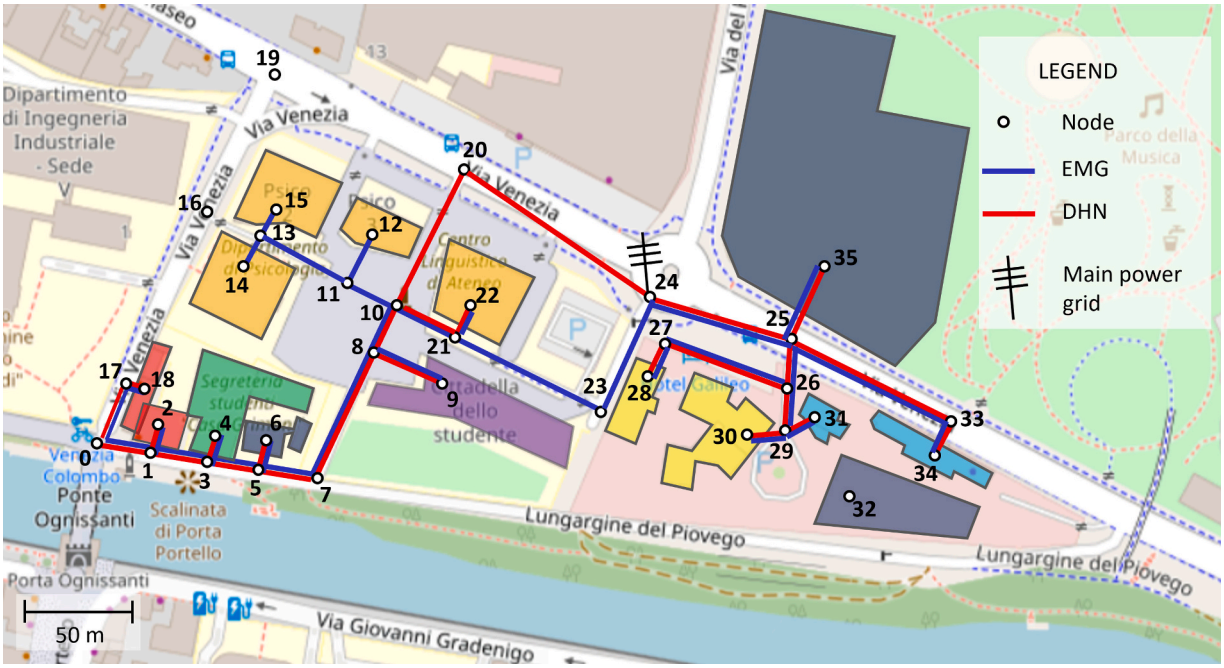

Fig. 5. Optimal layout of the considered MES, design from scratch.

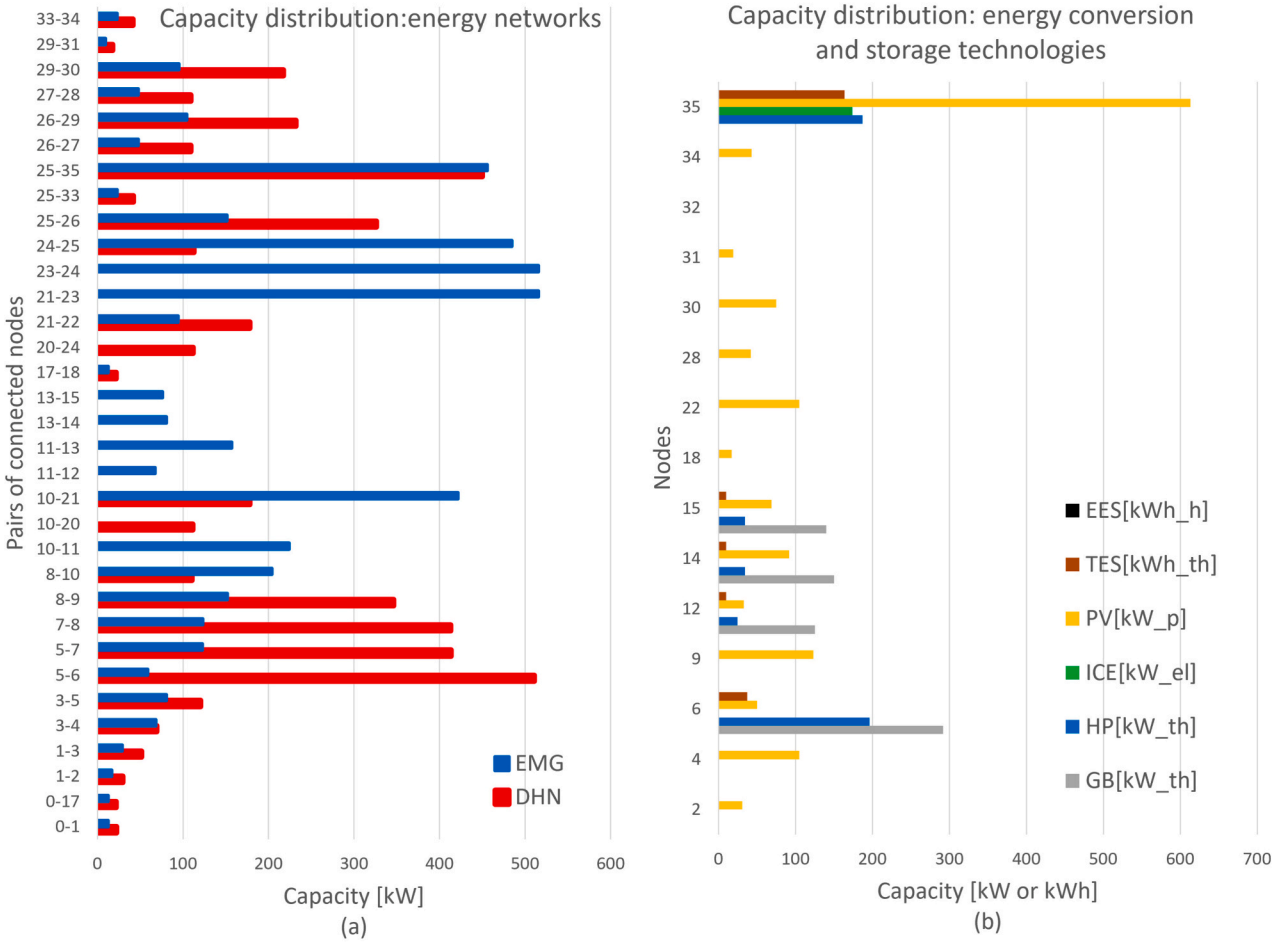

Fig. 6. Capacity distribution: (a) energy networks, (b) conversion and storage plants, design from scratch.

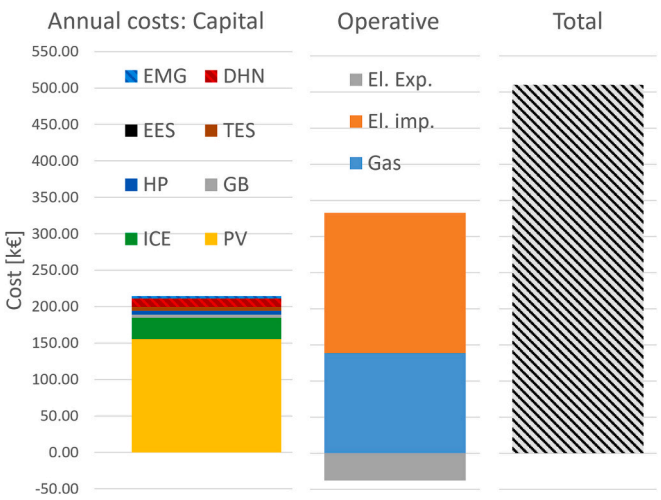

Fig. 7. Cost distribution of the optimal MES layout, design from scratch.

and the entire electricity demand with the main power grid. In this case, the annual costs and CO_2 emissions are 737.3 *k€* and 1277.6 *t*, respectively. Thus, the optimized MES results in a 31 % reduction in costs and 52 % reduction in emissions, suggesting that decarbonization is cost-effective at least up to a certain share of avoided CO_2 emissions. Note that no constraint is imposed here on CO_2 emissions. Thus, the decarbonization process is completely driven by cost-effectiveness in this case.

Fig. 7 shows how the total annual costs are distributed among the cost categories. Operating costs amount to 286.4 *k€*, of which 45 % is due to natural gas import. The remaining 55 % is due to electricity import net of exported electricity, the negative contribution of which is about 15 % of the total operating costs. Capital costs are 223.4 *k€*, with PV responsible for 64 % of the total. The second and third largest contributors to capital costs are ICE (12 %) and DHN (5 %). The limited impact of energy networks on capital costs is due to the small geographical extent of the system and the proximity of end users (the area under consideration is highly populated).

Fig. 8 shows the annual energy balances (electricity and heat), where each day of the year is replaced by the typical day representing it. PV is predominant in terms of supplied energy, especially during the summer period, with an annual production of 2055.9 *MWh* of renewable electricity, corresponding to 75 % of the total electricity generated on site. In contrast, CHP generation of the ICE is more prominent during the winter period. ICE produces 664.6 *MWh* of electricity annually, as if it were working 44 % of the year at rated power, and 814.3 *MWh* of heat, accounting for about 50 % of the annual demand. Note that the ICE is constrained to operate in CHP mode (it cannot release useful heat to the environment) in order to improve the overall efficiency of the system. The rest of the heat demand is almost entirely covered by HPs (807.4 *MWh/year* of thermal production, i.e., about 1700 equivalent hours at rated capacity per year), while GBs are used only to cover peaks (91.1 *MWh/year* of thermal production, i.e., less than 150 equivalent hours at rated capacity per year). Note that the DHN losses account for about 5 % of the total heat generated. Imported electricity is 767.2 *MWh/year* (30 % of demand), while exported electricity is 696.3 *MWh/year*, or 34 % of the electricity generated by PV. Overall, more than 70 % of electricity demand is covered by electricity generated locally.

4.2. Retrofit design

The retrofit design problem has been solved in about 2.5 h, reaching termination tolerance in 21 iterations. The shorter computation time compared with design from scratch is due to the fact that a larger number of binary synthesis variables has been fixed in advance, thus reducing the combinatorial complexity.

Fig. 9 shows the initial layout of energy networks and how it has changed after retrofit optimization. Accordingly, Fig. 10 shows (a) the initial distribution of network line capacity and how it has changed and (b) the mix of energy conversion and storage technologies before and

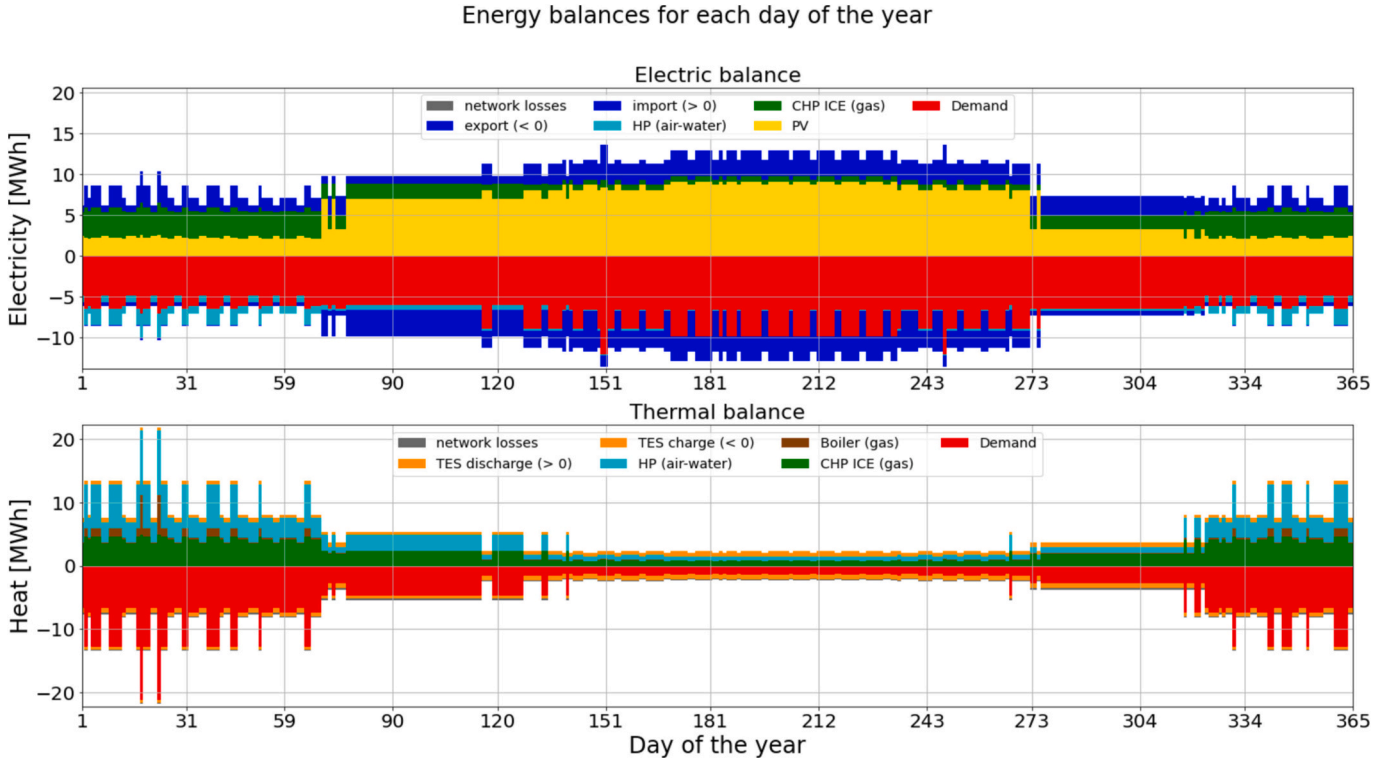

Fig. 8. Annual energy balances, design from scratch.

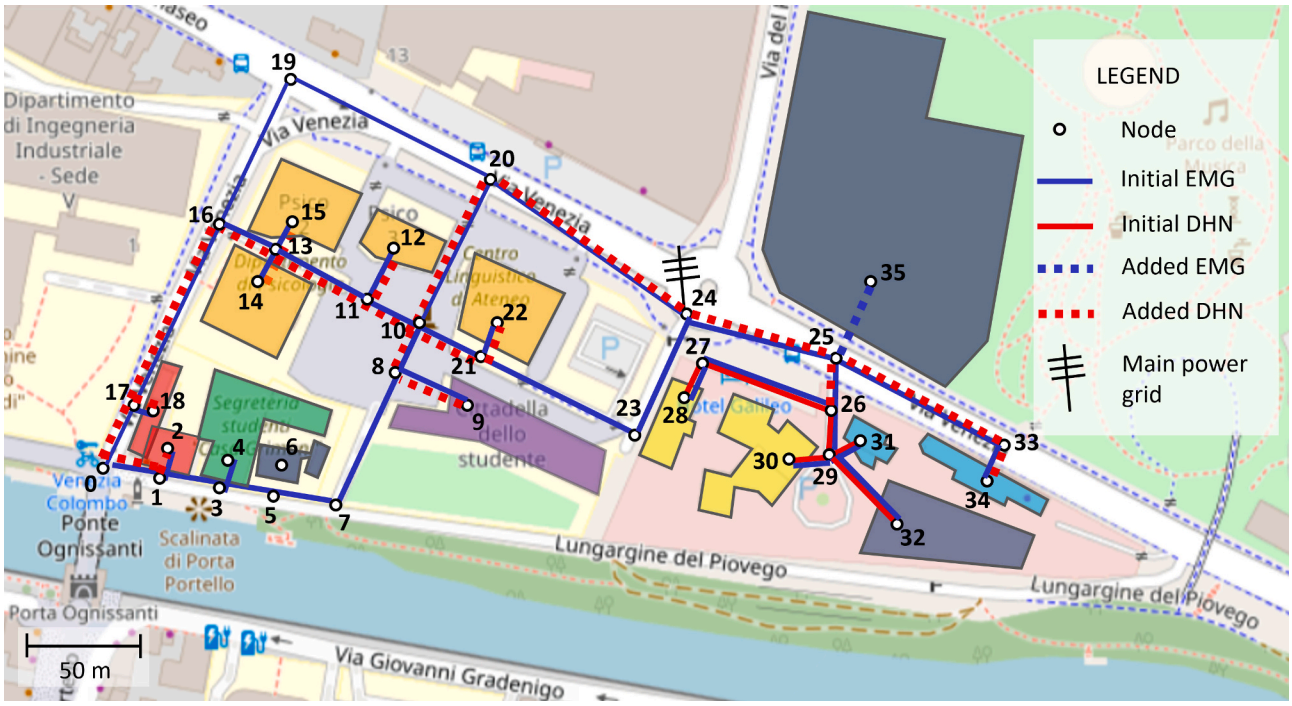

Fig. 9. Initial and optimal layout of the considered MES, retrofit design.

after the retrofit optimization. The initial layout of the EMG is meshed and connects all nodes except the energy hubs located at nodes 6 and 35. The initial layout of the DHN connects the energy hub located at node 32 to the end users at nodes 28, 30, and 31. The other users are independent in terms of heat demand, which they meet with GBs and/or HPs. In addition, some of them have availability of PV systems. The energy hub located at node 32 initially includes an ICE of 135 *kW* rated electrical power, a GB of 400 *kW* rated thermal power, and a TES of 100 *kWh* capacity. Regarding EMG, the optimized retrofit design results in the addition of the network line connecting node 25 to node 35, where an energy hub is located. That hub now includes a 561 kW_p PV plant, which is the largest in the system. PV plants with much lower capacities (below 150 kW_p) are also added in all nodes where they can be installed. DHN has been extended to all end-user buildings, with the exception of node 4, which is the most distant from the hubs and continues to meet its heat demand by GB. A HP of 222 *kW* nominal thermal power has been added to node 32 to meet the increased heat demand covered by DHN. In addition, 37 *kW* of rated electrical power has been added at the same hub to the already available ICE and 87 *kWh* of rated capacity to the already available TES. Finally, 10 *kWh* of rated capacity has been added to the 30 *kWh* of EES available at node 9. Note that the capacity of EES is still very limited, indicating that it is more cost-effective to provide the demand flexibility required by the system with other resources (such as PV coupled with HP and TES).

The annual cost associated with the initial configuration of the MES (before retrofit) is 577.3 *k€* and is composed of operating costs only, as the available plants and networks are considered to have been installed previously. The annual CO_2 emissions are 1047.8 *t*. The goal of retrofit design is to improve the performance of the MES by decreasing both the annual cost and the carbon emissions. As a result, the optimal annual cost after retrofit design is 439.6 *k€* and corresponds to a 24 % reduction, despite including capital costs. The resulting CO_2 emissions are 635.8 *t*, corresponding to a 39 % reduction. Note that no upper limit on carbon emissions is considered, so that the CO_2 reduction is determined only by cost-effectiveness.

Fig. 11 shows how the annual costs are distributed in the optimized MES layout. The operating costs account for 66 % of the total, with imported gas and electricity contributing almost equally (128 *k€/year* is due to natural gas, 144 *k€/year* is due to electricity import net of revenues for exported electricity). The capital costs are due to newly installed components and additional capacity. PV is the main contributor with 119 *k€*, accounting for 80 % of the total. The second largest contributor is DHN, with 6 *k€* (4 % of the total). The EMG contribution to capital costs is almost negligible because most of the network lines were already available in the starting configuration of the MES.

4.2.1. *Epsilon-constrained multi-objective optimization*

The proposed optimization method allows imposing a variable constraint on the maximum amount of CO_2 produced in order to perform a so-called "epsilon-constrained" multi-objective optimization between life-cycle cost minimization and emission minimization. Successively reducing ε in Eq. (31) means limiting CO_2 emissions to increasingly stringent targets. This results, for the retrofit problem, in the Pareto front shown in Fig. 12a. Further reductions in annual emissions compared to unconstrained optimization result in increased life-cycle costs, the two objectives being in conflict. Moreover, the relationship between the two objectives is not linear. Reducing emissions by 64 *t* from 636 *t* to 572 *t* increases the cost by 6 *k€*. In contrast, reducing emissions by the same amount from 447 *t* to 383 *t* increases the cost by 21 *k€*. Note that 383 *t/year* is the minimum limit of CO_2 produced. In fact, the emission reduction is mainly driven by increasing the installed capacity of PV and EES, as shown in Fig. 12b. However, PV capacity is upper limited by the area available for plant installation, thus limiting, in turn, the possible reduction of CO_2 produced. The increase in installed capacity of PV and EES is also the main cause of the cost increase on the Pareto front. A 40 % emission reduction (the maximum possible) requires installing an additional 1344 kW_p of PV (+100 %) and an additional 1270 *kWh* of EES (over 30 times more than the starting capacity).

Considering energy networks, the additional PV capacity installed to reduce carbon emissions requires upgrading the EMG. Specifically, the capacity of the line connecting nodes 24 and 25 grows from 570 *kW* when CO_2 emissions are not capped to 1307 *kW* (+130 %) when CO_2 emissions are reduced by 40 %. Moreover, the capacity of the line connecting nodes 25 and 35 grows from 439 to 1374 *kW* (+213 %) under the same conditions. These increases are justified by the fact that all the additional PV capacity (1344 kW_p) is installed at node 35. The

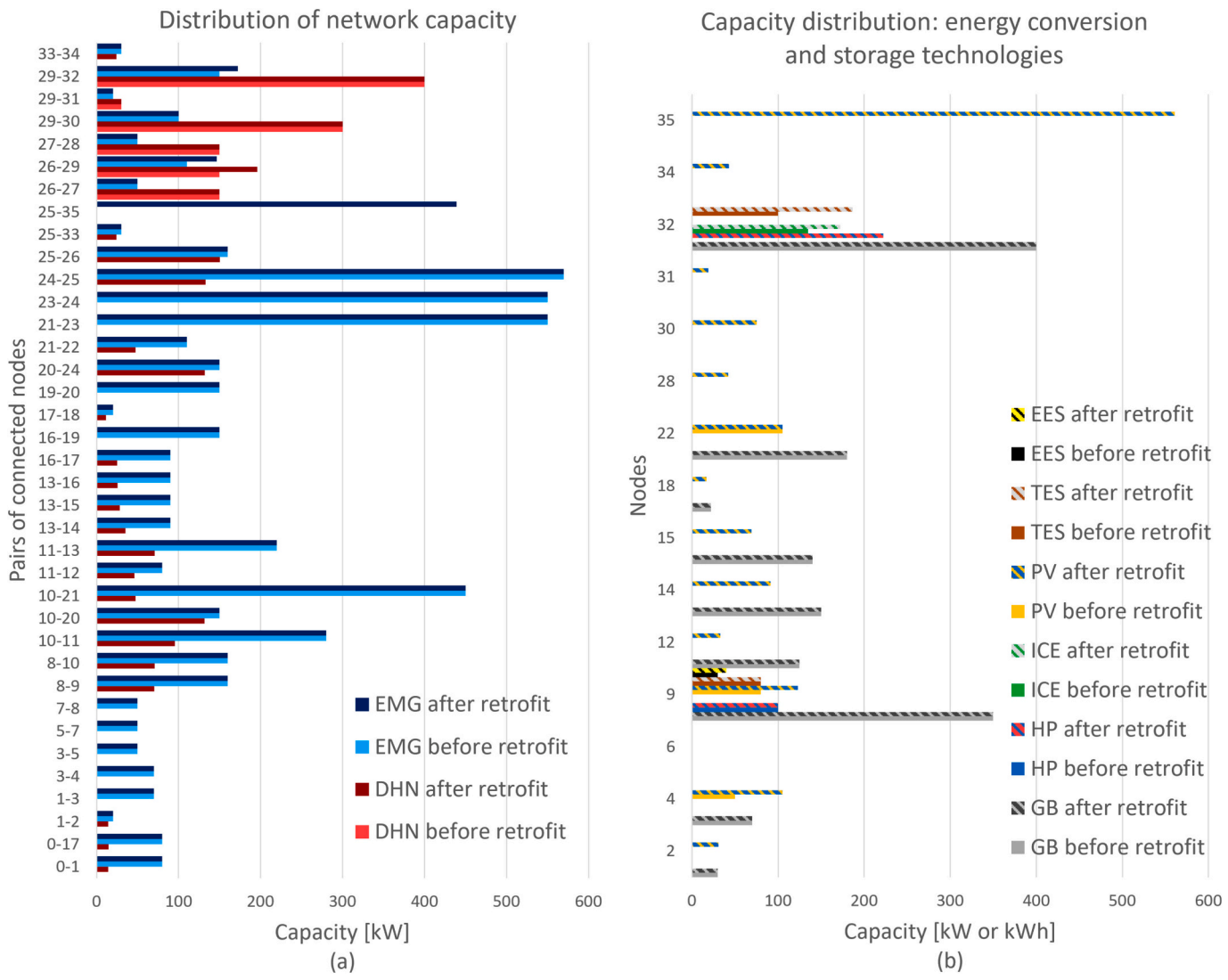

Fig. 10. Capacity distribution: (a) energy networks, (b) conversion and storage plants, retrofit design.

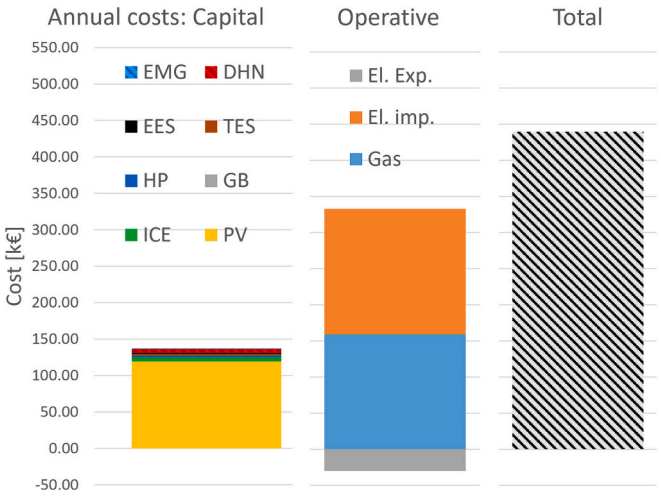

Fig. 11. Cost distribution of the optimal MES layout, retrofit design.

expanded EMG lines are in fact those connecting node 35 to the interface with the national grid at node 24 (see Fig. 9). DHN, on the other hand, undergoes only minor changes.

Fig. 12 shows also cost, emissions and capacities of the baseline system, i.e., the MES before retrofit. It is worth noting that, for this case study, even the most expensive configuration of the Pareto front is cheaper than the baseline, thereby highlighting the wide margin available to decarbonize the system.

5. Discussion

5.1. Choice of the number of typical days

One of the critical parameters that must be chosen properly to obtain reliable solutions of the SDO optimization problem is the number of representative TDs to be provided as input to the K-medoids algorithm for time series aggregation. Indeed, it is necessary to find a suitable compromise between (i) limiting the computational load and (ii) ensuring adequate accuracy of the solutions. In general, the higher the number of TDs, the more accurate the aggregated time series in representing annual ones, but the higher the computational requirements, which increase at least linearly with the total number of timesteps. In this study, 10 TDs have been chosen to represent the entire year, additionally including the two days of the year when the peaks for heat and electricity demands occur.

This choice has been validated by considering the “design from scratch” problem, which is the most time-consuming one. First, a MILP

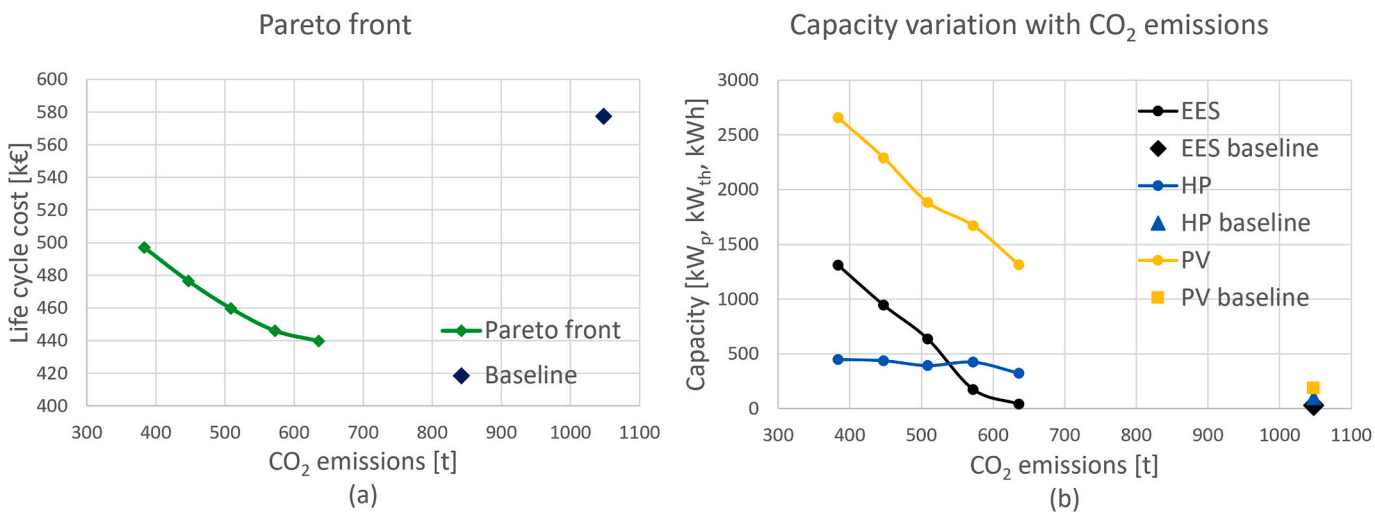

Fig. 12. (a) Pareto front between life cycle cost and CO_2 emissions, (b) capacity variation with emissions.

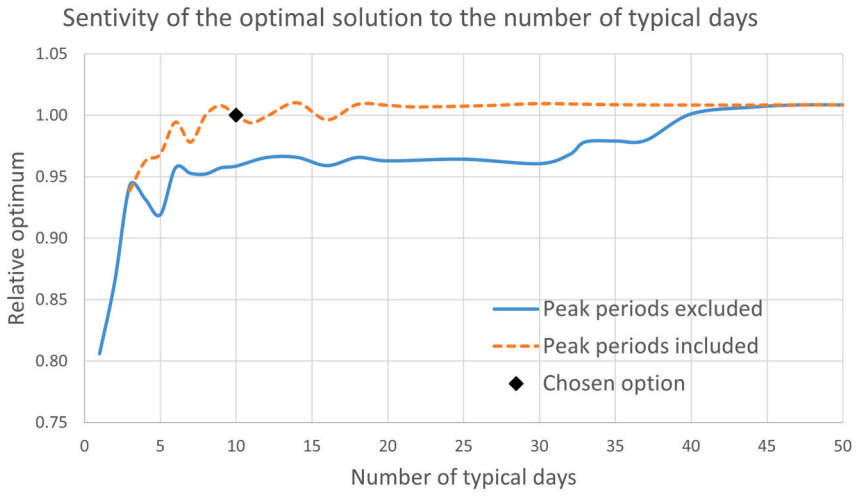

Fig. 13. Variation of the optimum (relative to design from scratch solution) with the number of typical days.

design and operation problem is set up by fixing the optimal synthesis variables obtained from the full SDO optimization problem described in Section 4.1. Then, the MILP problem is solved several times by progressively increasing the number of TDs obtained from the K-medoids algorithm by (i) not including the peak demand days and (ii) including the peak demand days. Fig. 13 shows the results of this analysis, where the relative optimum is the ratio between the value of the objective function obtained from the MILP design and operation subproblem and

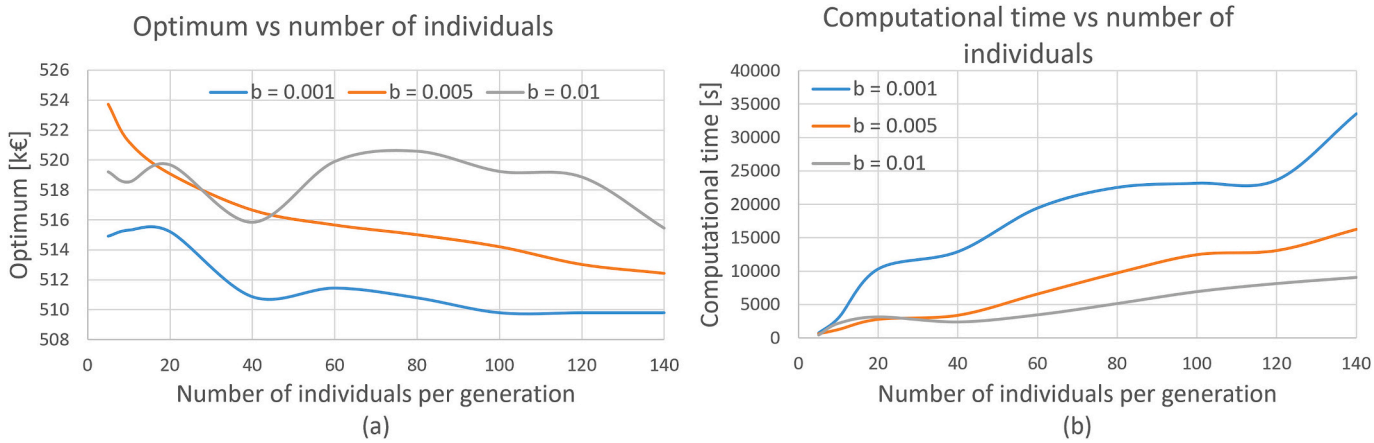

Fig. 14. Sensitivity analysis to the EA parameters "number of individuals" *a* and "termination tolerance" *b*: (a) value of the optimum, (b) computational time.

that obtained from the complete SDO problem. Note that a certain number of TDs is required for the optimum to reach stability. A very low number of TDs (2 to 5) leads to solutions that deviate up to 20 % from the stable optimum. The inclusion of peak periods allows the stable optimum to be reached with a lower number of TDs. In the range of 5 to 30 TDs, not including peaks means deviating from the stable optimum by about 4 % more than when including them. It can be seen that the chosen option (10 TDs peaks included) is still not in the stable region, which starts at about 20 TDs. However, the error with respect to the stable optimum is less than 1 %. This error is assumed to be acceptable, considering that using 20 TDs would mean at least doubling the computation time.

5.2. Validation of the evolutionary algorithm

The accuracy of the solution of the two-level EA depends on the parameters set by the user. Indeed, it is expected that, by increasing the number of individuals per generation and/or decreasing the termination tolerance, the solution gradually approaches the global optimum. If beyond certain threshold parameters the resulting value of the objective function stops changing, it is reasonable to assume that the obtained solution is "satisfactorily close" to the global optimum. To this end, a sensitivity analysis has been conducted on the EA parameters (number of individuals per generation a, termination tolerance b) considering the design from scratch problem, which is the most computationally demanding. Fig. 14 shows the results. A termination tolerance b of 0.01 or 0.005 is not sufficient to stabilize the optimum, even for a large number of individuals ($a > 100$). In contrast, by considering $b = 0.001$ the value of the optimum remains stable between 100 and 140 individuals per generation. Thus, it can be assumed with reasonable confidence that the optimal solution obtained imposing $b = 0.001$ and $a \geq 100$ (509.8 k€) is close to the global optimum. Accordingly, the parameters chosen in Section 3 ($a = 100, b = 0.001$) are consistent with reaching global optimality.

In general, the computation time increases as a increases and b decreases. It corresponds to 23,175 s, or 6.4 h, for $b = 0.001$ and $a = 100$. For the same number of individuals and $b = 0.005$, the computation time drops to 3.5 h, and the optimum deviates by less than 1 % from the supposed global optimum.

As discussed in Section 2.3.1, the previous validation is not a rigorous mathematical proof that the global optimum has been found, because the metaheuristic nature of two-level EA does not inherently guarantee global optimality. Global optimality can be achieved and proved mathematically by solving the complete SDO problem with a MILP approach, without decomposition. However, it is not possible to solve the considered case studies without decomposition because of to the limitations of available computational capacity. Thus, to strengthen the validation of the proposed method, a simpler test case including a smaller number of nodes has been considered. Due to the lower number of nodes, it is possible to solve the test case with a MILP approach without decomposing the problem. The global optimum obtained (global optimality is guaranteed by the MILP approach) is then compared with the solution obtained with the two-level DOMES algorithm for the same system.

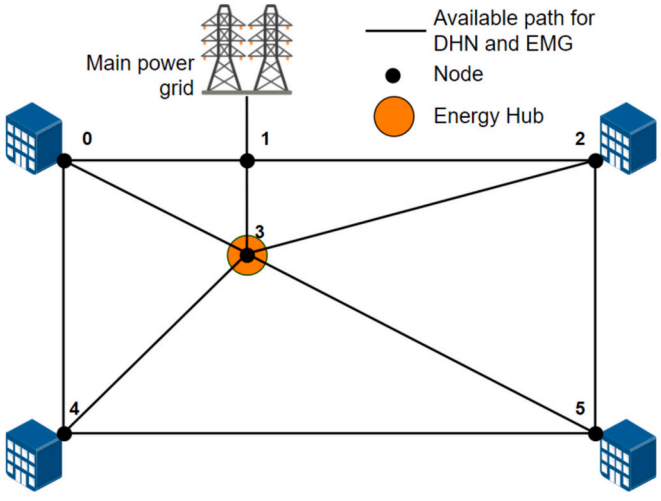

Fig. 15. Topology of the simplified test case.

Fig. 15 shows the simplified system topology of the considered test case. It consists of six nodes, four end users (multi-apartment residential buildings), an energy hub and is interconnected with the main power grid. PV, GB, HP, TES and EES can be installed at the end-user nodes, while an ICE (CHP unit), a GB and TES can be installed in the energy hub. The nodes can be connected via DHN and EMG. The objective function consists in minimizing the total annual costs for investment and operation. The techno-economic input data are the same as in the previous case studies, as shown in Tables 6–10. The same system location and weather data are also assumed.

The optimization of the test case is solved in about 3 h with the non-decomposed MILP approach and in about 3.5 h with the DOMES framework. In the first case, the value of the optimum is 234.4 $k€$ (this is the global optimum according to MILP features). In the second case, the value of the optimum is 235.7 $k€$ (+ 0.55 %). Thus, the gap between the two-level EA solution and the global optimum is less than 1 %. Table 11 shows the differences in the installed capacities of the considered technologies between the two optimization approaches. The differences are large when considering thermal power generators (GB, HP) and TES, with a peak of 28 % relative difference for GB. In all other cases the deviations are close to or less than 10 %. The effect of these deviations on the objective function is almost negligible, as shown by the gap between the achieved optima. This can be explained by the relatively low investment cost of technologies with larger deviations (especially GB and TES), which have a minor impact on the objective function.

5.3. Limitations of the proposed method

In order for the design and operation problem of a MES to be solved as MILP in the lower level of the EA, some modelling simplifications need to be made. In particular, off-design maps of dispatchable energy conversion technologies have been linearized between nominal capacity and minimum load conditions. This approximation is acceptable for most technologies, since they show a fairly linear behaviour under off-design conditions. However, linearization introduces some distortions into the results. Thus, some precautions have been taken to limit these distortions as much as possible. First, linearization concerns the relationship between the "fuel" and the "product" of the conversion unit. Because of the known term in the linear equation, the efficiency (defined as the product/fuel ratio) is not linear with the product, showing a steeper decrease at lower partial loads, as expected for real systems. Second, the part-load operation of the components is limited to a narrow

Table 11
Installed capacity of the considered technologies, emissions and resulting value of the objective function in the test case: comparison between non-decomposed MILP problem and the DOMES algorithm.

Technology	MILP	DOMES	Gap [%]
PV [kW_p]	524.1	474.3	−10.5
ICE [kW_{el}]	103.4	102.3	−1.1
GB [kW_{th}]	186.3	260.2	+28.4
HP [kW_{th}]	277.3	238.2	−16.4
TES [kWh]	174.1	154.7	−12.5
EMG [kW_{el}.km]	56.4	53.5	−5.5
DHN [kW_{th}.km]	55.1	57.1	+3.4
Annual CO_2 emissions [t]	306.2	312.9	+2.1
Objective function [k€]	234.4	235.7	+0.55

range in which the efficiency varies only slightly (e.g., CHP units operate in the range of 100 % to 70 % of rated load). This choice preserves the efficient and safe operation of the components, as commonly occurs in real applications. Note also that the inclusion of nonlinear constraints to better model off-design conditions would require more sophisticated optimization techniques (capable of handling nonconvexity) and, in turn, significantly higher computational effort. An alternative to keep the model linear while better modelling the nonlinearities is piecewise linearization. In practice, nonlinear curves would be approximated by linear segments. However, an additional binary variable must be added to the model for each segment, thus exponentially increasing the computational requirements.

The model of energy networks has also been linearized. Namely, only power flows within network lines are modelled here, assuming the other operational parameters as constants. This is a recognized approach in the literature for topological optimization. For instance, Röder et al. [50] assumed constant supply and return temperatures and pressure levels in the topological optimization of a DHN. In this way, heat transport in the network is directly proportional to the circulating mass flow rate, and pipelines can be sized according to their maximum mass flow rate (i.e., maximum thermal power that can be transferred). The same approach is followed here. A similar approach has also been chosen for EMG. In this case, the node voltages have been set as constant values. The power transferred is therefore directly proportional to the electric current, which is the sizing parameter.

Because of the above-mentioned simplifications, DOMES is intended for the preliminary planning and design phase of a MES. It can provide useful guidance to decision makers on how to plan a system to minimize cost and/or reduce carbon emissions, while providing an overall picture of the system performances. This justifies the assumed simplifications. More detailed simulations, including nonlinear behaviours, can be run on specific parts of the system to gain insights.

Moreover, the proposed method does not evaluate how uncertainty in the input data (demand profiles, investment costs, energy carrier prices, resource availability, etc.) affects the results. A sensitivity analysis is out of the scope of this paper, which focuses on describing the optimization methodology. However, as a further development, uncertainties could be taken into account by means of stochastic programming techniques. This approach would maintain the linearity of the model, which would still be treated as MILP, but would increase computational complexity due to the consideration of different probabilistic scenarios.

Finally, the EA described here has so far been tested only on MESs of limited spatial extent. How expanding the geographic area and number of nodes may affect the practicality of finding the global optimum requires further investigation. Some guidance is provided by comparing the test case and the case study related to design from scratch. The MES of the first case includes 6 nodes and is solved in 3.5 *h*. The second one contains 36 nodes and is solved in 6 *h*. This suggests that the number of nodes can be further increased without compromising computational feasibility. However, larger systems with hundreds or thousands of nodes would not be solvable in acceptable time. Thus, the DOMES framework can be scaled to larger geographic areas, provided that the number of nodes is kept small enough (the larger the system, the lower the spatial resolution). One possibility for modelling large systems while keeping the number of nodes small is to apply clustering techniques not only for time series aggregation, but also for spatial aggregation.

6. Conclusions

This paper presents "*DOMES*" (acronym for Design Of Multi-Energy Systems), a general optimization method for the integrated synthesis, design and operation (SDO) of a multi-energy system (MES) in its entirety. It simultaneously identifies the type, size, location, and scheduling of energy conversion and storage units, along with the topology and capacity of the energy networks, to fulfil the energy demands of the end users. For this purpose, an evolutionary algorithm has been developed. It decomposes the entire SDO problem into two levels with the aim of reducing the computational complexity, which would otherwise make the problem unsolvable within a reasonable time frame. Most of the binary decision variables are thus isolated in the upper level, which defines the system topology, while the lower level optimizes the size and operation of the included components with a mixed integer linear programming (MILP) approach.

The case study considered has demonstrated the ability of DOMES to address both the "design from scratch" of new MESs and the "retrofit design" of existing ones. The design from scratch problem has been solved in about six hours of computation and the retrofit problem in less than three hours by using a common computer. The computation times are therefore acceptable compared to the complexity of the problem and demonstrate the effectiveness of the proposed two-level algorithm in optimizing the SDO of a MES. In addition, the accuracy of the obtained solutions has been verified by sensitivity analysis on user-settable parameters of the evolutionary algorithm. It has been demonstrated with reasonable confidence that the proposed optimization method is able to find the global optimum of the problem that would be achieved without decomposition.

Considering a district MES located in Padova, Italy, the optimal system configuration resulting from retrofit design reduces annual costs by 25 % and CO_2 emissions by 40 % compared to the original system layout. This share of avoided CO_2 emissions is determined exclusively by cost-effectiveness, thus demonstrating the wide margin available to decarbonize current energy systems. CO_2 emissions can be further reduced by 40 % if multi-objective optimization is carried out, with annual costs concurrently increasing by less than 15 %. The electrical microgrid makes it possible to cover more than 70 % of the electricity demand with energy generated on-site from photovoltaic (PV) panels and combined heat and power internal combustion engines. In general, the coupling of PV with heat pumps and thermal energy storage turns out to be a crucial source of flexibility to decarbonize heat demand, which is in fact covered about 50 % by PV-powered heat pumps and the rest almost entirely by cogenerated heat. PV dominates in investment costs with 80 % of the total, while the second largest contribution of about 5 % comes from district heating. Less than 10 % of the total investment is due to district heating network and electric microgrid together. However, the consideration of an urban district is an extreme case that suggests a much higher economic impact of energy networks when considering larger and less densely populated areas.

It is worth emphasizing again that some simplifications, such as linearization, problem decomposition, and time series aggregation, are required to make the SDO problem of a MES computationally solvable, at the expense of slightly reducing the accuracy of the results. However, these simplifications are necessary to find a solution to the problem that, although improvable, is the only one that can be practically achieved.

In conclusion, DOMES can provide decision makers with useful information on how to properly plan, design, and schedule local MESs to meet increasingly stringent decarbonization targets. The possible inclusion of other networks (e.g., gas network, cooling network), as well as the enlargement of the spatial extent of the MES, would not alter the general approach proposed here, which can handle also more complex systems provided that sufficient "computing power" is available.

CRediT authorship contribution statement

Enrico Dal Cin: Writing – original draft, Software, Methodology, Formal analysis, Conceptualization. **Gianluca Carraro:** Writing – review & editing, Software, Methodology, Conceptualization. **Gabriele Volpato:** Writing – review & editing, Formal analysis. **Andrea Lazzaretto:** Writing – review & editing, Supervision, Conceptualization. **George Tsatsaronis:** Writing – review & editing, Supervision, Conceptualization.

Declaration of competing interest

The authors declare that they have no known competing financial interests or personal relationships that could have appeared to influence the work reported in this paper.

Data availability

Data will be made available on request.

Acknowledgment

This research did not receive any specific grant from funding agencies in the public, commercial, or not-for-profit sectors.

References

[1] ClimateWatch. Historical GHG emissions. https://www.climatewatchdata.org/ghg-emissions?source=Climate%20Watch.
[2] United Nations. The Paris agreement. https://unfccc.int/process-and-meetings/the-paris-agreement/the-paris-agreement; 2015.
[3] Cap S, de Koning A, Tukker A, Scherer L. (in)sufficiency of industrial decarbonization to reduce household carbon footprints to 1.5°C-compatible levels. Sustain Prod Consump 2024;45:216–27. https://doi.org/10.1016/j.spc.2023.12.031.
[4] Papadis E, Tsatsaronis G. Challenges in the decarbonization of the energy sector. Energy 2020;205:118025. https://doi.org/10.1016/j.energy.2020.118025.
[5] Lund H, Østergaard PA, Connolly D, Mathiesen BV. Smart energy and smart energy systems. Energy 2017;137:556–65. https://doi.org/10.1016/j.energy.2017.05.123.
[6] Alabi TM, Agbajor FD, Yang Z, Lu L, Ogungbile AJ. Strategic potential of multi-energy system towards carbon neutrality: a forward-looking overview. Energy Built Environ 2023;4:689–708. https://doi.org/10.1016/j.enbenv.2022.06.007.
[7] Mancarella P. MES (multi-energy systems): an overview of concepts and evaluation models. Energy 2014;65:1–17. https://doi.org/10.1016/j.energy.2013.10.041.
[8] Xu Y, Yan C, Liu H, Wang J, Yang Z, Jiang Y. Smart energy systems: a critical review on design and operation optimization. Sustain Cities Soc 2020;62:102369. https://doi.org/10.1016/j.scs.2020.102369.
[9] Frangopoulos C, von Spakovsky M, Sciubba E. A brief review of methods for the design and synthesis optimization of energy systems. Int J Thermodyn 2002;5. https://doi.org/10.5541/ijot.97.
[10] Wang L, Yang Z, Sharma S, Mian A, Lin T-E, Tsatsaronis G, et al. A review of evaluation, optimization and synthesis of energy systems: methodology and application to thermal power plants. Energies 2019;12. https://doi.org/10.3390/en12010073.
[11] Toffolo A. A synthesis/design optimization algorithm for Rankine cycle based energy systems. Energy 2014;66:115–27. https://doi.org/10.1016/j.energy.2014.01.070.
[12] Wang L, Lampe M, Voll P, Yang Y, Bardow A. Multi-objective superstructure-free synthesis and optimization of thermal power plants. Energy 2016;116:1104–16. https://doi.org/10.1016/j.energy.2016.10.007.
[13] Wang L, Voll P, Lampe M, Yang Y, Bardow A. Superstructure-free synthesis and optimization of thermal power plants. Energy 2015;91:700–11. https://doi.org/10.1016/j.energy.2015.08.068.
[14] Olsommer B, Favrat D, Von Spakovsky M. An approach for the time-dependent Thermoeconomic modeling and optimization of energy system synthesis, design and operation part I: Methodology and results. Int J Thermodyn 1999;2:97–114.
[15] Olsommer B, Favrat D, Von Spakovsky M. An approach for the time-dependent Thermoeconomic modeling and optimization of energy system synthesis, design and operation part II: Reliability and availability. Int J Thermodyn 1999;2:177–86.
[16] Dal Cin E, Lazzaretto A, Toffolo A. A novel extension of the SYNTHSEP methodology for the optimal synthesis and design of supercritical CO2 cycles in waste heat recovery applications. Energy Convers Manag 2023;276:116535. https://doi.org/10.1016/j.enconman.2022.116535.
[17] Lazzaretto A, Manente G, Toffolo A. SYNTHSEP: a general methodology for the synthesis of energy system configurations beyond superstructures. Energy 2018;147:924–49. https://doi.org/10.1016/j.energy.2018.01.075.
[18] Lazzaretto A, Toffolo A. A practical tool to generate complex energy system configurations based on the SYNTHSEP methodology. Int J Thermodyn 2019;22:45–53. https://doi.org/10.5541/ijot.506382.
[19] Toffolo A, Rech S, Lazzaretto A. Generation of complex energy systems by combination of elementary processes. J Energy Resour Technol 2018;140. https://doi.org/10.1115/1.4040194.
[20] Elsido C, Mian A, Martelli E. A systematic methodology for the techno-economic optimization of organic Rankine cycles. Energy Procedia 2017;129:26–33. https://doi.org/10.1016/j.egypro.2017.09.171.
[21] MuÑOz J, Von Spakovsky M. The application of decomposition to the large scale synthesis/design optimization of aircraft energy systems. Int J Thermodyn 2001;4:61–76.
[22] Dimopoulos GG, Kougioufas AV, Frangopoulos CA. Synthesis, design and operation optimization of a marine energy system. Energy 2008;33:180–8. https://doi.org/10.1016/j.energy.2007.09.004.
[23] Sakalis GN, Frangopoulos CA. Intertemporal optimization of synthesis, design and operation of integrated energy systems of ships: general method and application on a system with diesel main engines. Appl Energy 2018;226:991–1008. https://doi.org/10.1016/j.apenergy.2018.06.061.
[24] Sakalis GN, Tzortzis GJ, Frangopoulos CA. Intertemporal static and dynamic optimization of synthesis, design, and operation of integrated energy systems of ships. Energies 2019;12. https://doi.org/10.3390/en12050893.
[25] Voll P, Lampe M, Wrobel G, Bardow A. Superstructure-free synthesis and optimization of distributed industrial energy supply systems. Energy 2012;45:424–35. https://doi.org/10.1016/j.energy.2012.01.041.
[26] Hennen M, Postels S, Voll P, Lampe M, Bardow A. Multi-objective synthesis of energy systems: efficient identification of design trade-offs. Comput Chem Eng 2017;97:283–93. https://doi.org/10.1016/j.compchemeng.2016.10.010.
[27] Algieri A, Beraldi P, Pagnotta G, Spadafora I. The optimal design, synthesis and operation of polygeneration energy systems: balancing life cycle environmental and economic priorities. Energy Convers Manag 2021;243:114354. https://doi.org/10.1016/j.enconman.2021.114354.
[28] Testi D, Conti P, Schito E, Urbanucci L, D'Ettorre F. Synthesis and optimal operation of smart microgrids serving a cluster of buildings on a campus with centralized and distributed hybrid renewable energy units. Energies 2019;12. https://doi.org/10.3390/en12040745.
[29] Mancò G, Tesio U, Guelpa E, Verda V. A review on multi energy systems modelling and optimization. Appl Therm Eng 2024;236:121871. https://doi.org/10.1016/j.applthermaleng.2023.121871.
[30] Frangopoulos CA. Recent developments and trends in optimization of energy systems. Energy 2018;164:1011–20. https://doi.org/10.1016/j.energy.2018.08.218.
[31] Rech S. Smart energy systems: guidelines for modelling and optimizing a Fleet of units of different configurations. Energies 2019;12:1320. https://doi.org/10.3390/en12071320.
[32] Rao SS. Integer programming. In: Engineering Optimization Theory and Practice; 2019. p. 537–74. https://doi.org/10.1002/9781119454816.ch10.
[33] Urbanucci L. Limits and potentials of mixed integer linear programming methods for optimization of polygeneration energy systems. Energy Procedia 2018;148:1199–205. https://doi.org/10.1016/j.egypro.2018.08.021.
[34] Marquant JF, Evins R, Bollinger LA, Carmeliet J. A holarchic approach for multi-scale distributed energy system optimisation. Appl Energy 2017;208:935–53. https://doi.org/10.1016/j.apenergy.2017.09.057.
[35] Dal Cin E, Carraro G, Volpato G, Lazzaretto A, Danieli P. A multi-criteria approach to optimize the design-operation of energy communities considering economic-environmental objectives and demand side management. Energy Convers Manag 2022;263:115677. https://doi.org/10.1016/j.enconman.2022.115677.
[36] Volpato G, Carraro G, Cont M, Danieli P, Rech S, Lazzaretto A. General guidelines for the optimal economic aggregation of prosumers in energy communities. Energy 2022;258:124800. https://doi.org/10.1016/j.energy.2022.124800.
[37] Rech S, Lazzaretto A. Smart rules and thermal, electric and hydro storages for the optimum operation of a renewable energy system. Energy 2018;147:742–56. https://doi.org/10.1016/j.energy.2018.01.079.
[38] Bracco S, Delfino F, Ferro G, Pagnini L, Robba M, Rossi M. Energy planning of sustainable districts: towards the exploitation of small size intermittent renewables in urban areas. Appl Energy 2018;228:2288–97. https://doi.org/10.1016/j.apenergy.2018.07.074.
[39] Guo J, Zhang P, Wu D, Liu Z, Liu X, Zhang S, et al. Multi-objective optimization design and multi-attribute decision-making method of a distributed energy system based on nearly zero-energy community load forecasting. Energy 2022;239:122124. https://doi.org/10.1016/j.energy.2021.122124.
[40] Wirtz M. nPro: a web-based planning tool for designing district energy systems and thermal networks. Energy 2023;268:126575. https://doi.org/10.1016/j.energy.2022.126575.
[41] Wirtz M, Heleno M, Moreira A, Schreiber T, Müller D. 5th generation district heating and cooling network planning: A Dantzig–Wolfe decomposition approach. Energy Convers Manag 2023;276:116593. https://doi.org/10.1016/j.enconman.2022.116593.
[42] Mashayekh S, Stadler M, Cardoso G, Heleno M. A mixed integer linear programming approach for optimal DER portfolio, sizing, and placement in multi-energy microgrids. Appl Energy 2017;187:154–68. https://doi.org/10.1016/j.apenergy.2016.11.020.
[43] Morvaj B, Evins R, Carmeliet J. Optimization framework for distributed energy systems with integrated electrical grid constraints. Appl Energy 2016;171:296–313. https://doi.org/10.1016/j.apenergy.2016.03.090.
[44] Nazari-Heris M, Mohammadi-Ivatloo B, Asadi S. Optimal operation of multi-carrier energy networks with gas, power, heating, and water energy sources considering different energy storage technologies. J Energy Storage 2020;31:101574. https://doi.org/10.1016/j.est.2020.101574.
[45] Tesio U, Guelpa E, Verda V. Including thermal network operation in the optimization of a multi energy system. Energy Convers Manag 2023;277:116682. https://doi.org/10.1016/j.enconman.2023.116682.
[46] Wang J, Lei T, Qi X, Zhao L, Liu Z. Chance-constrained optimization of distributed power and heat storage in integrated energy networks. J Energy Storage 2022;55:105662. https://doi.org/10.1016/j.est.2022.105662.
[47] Danieli P, Carraro G, Volpato G, Cin ED, Lazzaretto A, Masi M. Guidelines for minimum cost transition planning to a 100% renewable multi-regional energy

system. Appl Energy 2024;357:122497. https://doi.org/10.1016/j.apenergy.2023.122497.
[48] Danieli P, Masi M, Lazzaretto A, Carraro G, Dal Cin E, Volpato G. Is banning fossil-fueled internal combustion engines the first step in a realistic transition to a 100% RES share? Energies 2023;16. https://doi.org/10.3390/en16155690.
[49] Pizzolato A, Sciacovelli A, Verda V. Topology optimization of Robust District heating networks. J Energy Resour Technol 2017;140. https://doi.org/10.1115/1.4038312.
[50] Röder J, Meyer B, Krien U, Zimmermann J, Stührmann T, Zondervan E. Optimal design of district heating networks with distributed thermal energy storages – method and case study. Int J Sustain Energy Plann Manage 2021;31:5–22. https://doi.org/10.5278/ijsepm.6248.
[51] Lambert RSC, Maier S, Shah N, Polak JW. Optimal phasing of district heating network investments using multi-stage stochastic programming. Int J Sustain Energy Plann Manage 2016;9:57–74. https://doi.org/10.5278/ijsepm.2016.9.5.
[52] Delangle A, Lambert RSC, Shah N, Acha S, Markides CN. Modelling and optimising the marginal expansion of an existing district heating network. Energy 2017;140:209–23. https://doi.org/10.1016/j.energy.2017.08.066.
[53] Söderman J, Pettersson F. Structural and operational optimisation of distributed energy systems. Appl Therm Eng 2006;26:1400–8. https://doi.org/10.1016/j.applthermaleng.2005.05.034.
[54] Haikarainen C, Pettersson F, Saxén H. A model for structural and operational optimization of distributed energy systems. Appl Therm Eng 2014;70:211–8. https://doi.org/10.1016/j.applthermaleng.2014.04.049.
[55] Keirstead J, Samsatli N, Shah N, Weber C. The impact of CHP (combined heat and power) planning restrictions on the efficiency of urban energy systems. Energy 2012;41:93–103. https://doi.org/10.1016/j.energy.2011.06.011.
[56] Mehleri ED, Sarimveis H, Markatos NC, Papageorgiou LG. A mathematical programming approach for optimal design of distributed energy systems at the neighbourhood level. Energy 2012;44:96–104. https://doi.org/10.1016/j.energy.2012.02.009.
[57] Omu A, Choudhary R, Boies A. Distributed energy resource system optimisation using mixed integer linear programming. Energy Policy 2013;61:249–66. https://doi.org/10.1016/j.enpol.2013.05.009.
[58] Weber C, Shah N. Optimisation based design of a district energy system for an eco-town in the United Kingdom. Energy 2011;36:1292–308. https://doi.org/10.1016/j.energy.2010.11.014.
[59] Mehleri ED, Sarimveis H, Markatos NC, Papageorgiou LG. Optimal design and operation of distributed energy systems: application to Greek residential sector. Renew Energy 2013;51:331–42. https://doi.org/10.1016/j.renene.2012.09.009.
[60] Yang Y, Zhang S, Xiao Y. Optimal design of distributed energy resource systems coupled with energy distribution networks. Energy 2015;85:433–48. https://doi.org/10.1016/j.energy.2015.03.101.
[61] Sidnell T, Clarke F, Dorneanu B, Mechleri E, Arellano-Garcia H. Optimal design and operation of distributed energy resources systems for residential neighbourhoods. Smart Energy 2021;4:100049. https://doi.org/10.1016/j.segy.2021.100049.
[62] Bracco S, Dentici G, Siri S. Economic and environmental optimization model for the design and the operation of a combined heat and power distributed generation system in an urban area. Energy 2013;55:1014–24. https://doi.org/10.1016/j.energy.2013.04.004.
[63] Casisi M, Pinamonti P, Reini M. Optimal lay-out and operation of combined heat & power (CHP) distributed generation systems. Energy 2009;34:2175–83. https://doi.org/10.1016/j.energy.2008.10.019.
[64] Fazlollahi S, Becker G, Maréchal F. Multi-objectives, multi-period optimization of district energy systems: III. Distribution networks. Comput Chem Eng 2014;66:82–97. https://doi.org/10.1016/j.compchemeng.2014.02.018.
[65] Girardin L, Marechal F, Dubuis M, Calame-Darbellay N, Favrat D. EnerGis: a geographical information based system for the evaluation of integrated energy conversion systems in urban areas. Energy 2010;35:830–40. https://doi.org/10.1016/j.energy.2009.08.018.
[66] Lerbinger A, Petkov I, Mavromatidis G, Knoeri C. Optimal decarbonization strategies for existing districts considering energy systems and retrofits. Appl Energy 2023;352:121863. https://doi.org/10.1016/j.apenergy.2023.121863.
[67] Morvaj B, Evins R, Carmeliet J. Optimising urban energy systems: simultaneous system sizing, operation and district heating network layout. Energy 2016;116:619–36. https://doi.org/10.1016/j.energy.2016.09.139.
[68] Comodi G, Bartolini A, Carducci F, Nagaranjan B, Romagnoli A. Achieving low carbon local energy communities in hot climates by exploiting networks synergies in multi energy systems. Appl Energy 2019;256:113901. https://doi.org/10.1016/j.apenergy.2019.113901.
[69] Casisi M, Costanzo S, Pinamonti P, Reini M. Two-level evolutionary multi-objective optimization of a district heating system with distributed cogeneration. Energies 2019;12. https://doi.org/10.3390/en12010114.
[70] Dos Santos KV, Santos L Higino Silva, Arias N Bañol, López JC, Rider MJ, Da Silva LCP. Optimal sizing and allocation of distributed energy resources in microgrids considering internal network reinforcements. J Control Autom Electr Syst 2023;34:106–19. https://doi.org/10.1007/s40313-022-00934-x.
[71] Dal Cin E, Carraro G, Lazzaretto A, Tsatsaronis G. Optimizing the retrofit design and operation of multi-energy systems integrated with energy networks. J Energy Resour Technol 2024;146. https://doi.org/10.1115/1.4064473.
[72] Rieder A, Christidis A, Tsatsaronis G. Multi criteria dynamic design optimization of a small scale distributed energy system. Energy 2014;74:230–9. https://doi.org/10.1016/j.energy.2014.06.007.
[73] Hoffmann M, Kotzur L, Stolten D, Robinius M. A review on time series aggregation methods for energy system models. Energies 2020;13. https://doi.org/10.3390/en13030641.
[74] MuÑOz J, Von Spakovsky M. A decomposition approach for the large scale synthesis design optimization of highly coupled, highly dynamic energy systems. Int J Thermodyn 2000;4:19–33.
[75] Kotzur L, Markewitz P, Robinius M, Stolten D. Impact of different time series aggregation methods on optimal energy system design. Renew Energy 2018;117:474–87. https://doi.org/10.1016/j.renene.2017.10.017.
[76] Glover F. Improved linear integer programming formulations of nonlinear integer problems. Manag Sci 1975;22:455–60.
[77] Kotzur L, Markewitz P, Robinius M, Stolten D. Time series aggregation for energy system design: modeling seasonal storage. Appl Energy 2018;213:123–35. https://doi.org/10.1016/j.apenergy.2018.01.023.
[78] Yang X-S. Chapter 14 - multi-objective optimization. In: Yang X-S, editor. Nature-Inspired Optimization Algorithms. Oxford: Elsevier; 2014. p. 197–211. https://doi.org/10.1016/B978-0-12-416743-8.00014-2.
[79] Yang X-S. Chapter 6 - genetic algorithms. In: Nature-Inspired Optimization Algorithms. 2nd ed. 2021. p. 91–100. https://doi.org/10.1016/B978-0-12-821986-7.00013-5.
[80] European Commission. Photovoltaic geographical information system (PVGIS). https://re.jrc.ec.europa.eu/pvg_tools/it/#MR; 2024.
[81] Dal Cin E, Carraro G, Lazzaretto A, Tsatsaronis G, Volpato G, Danieli P. Integrated design and operation optimization of multi-energy systems including energy networks. In: 36th International Conference on Efficiency, Cost, Optimization, Simulation and Environmental Impact of Energy Systems (ECOS 2023); 2023. p. 3362–73 (12 pages), 10.52202/069564-0302.
[82] Danish Energy Agency. Technology Data. https://ens.dk/en/our-services/projections-and-models/technology-data; 2023.
[83] Sterchele P, Brandes J, Heilig J, Wrede D, Kost C, Schlegl T, et al. Paths to a Climate-Neutral Energy System. The German Energy Transition in its Social Context. Fraunhofer ISE; 2020. https://www.ise.fraunhofer.de/en/publications/studies/paths-to-a-climate-neutral-energy-system.html.
[84] DESTATIS - Statisches Bundesmat. Data on energy price trends - Long-time series to Dezember 2022. https://www.destatis.de/EN/Themes/Economy/Prices/Publications/Downloads-Energy-Price-Trends/energy-price-trends-pdf-5619002.html; 2023.
[85] GME. Dati storici MGP. https://www.mercatoelettrico.org/it/download/DatiStorici.aspx; 2024.